Combined analysis of η meson hadro- and photo-production off nucleons

K. Nakayama,[1,2,*] Yongseok Oh,[3,†] and H. Haberzettl[4,‡]

[1] *Department of Physics and Astronomy, University of Georgia, Athens, GA 30602, U.S.A.*
[2] *Institut für Kernphysik (Theorie), Forschungszentrum Jülich, 52425 Jülich, Germany*
[3] *Cyclotron Institute, Texas A&M University, College Station, TX 77843, U.S.A.*
[4] *Center for Nuclear Studies, Department of Physics, The George Washington University, Washington, DC 20052, U.S.A.*

(Dated: 30 March 2008)

The η-meson production in photon- and hadron-induced reactions, namely, $\gamma p \to p\eta$, $\pi^- p \to n\eta$, $pp \to pp\eta$, and $pn \to pn\eta$, are investigated in a combined analysis in order to learn about the relevant production mechanisms and the possible role of nucleon resonances in these reactions. We consider the nucleonic, mesonic, and nucleon resonance currents constructed within an effective Lagrangian approach and compare the results with the available data for cross sections and spin asymmetries for these reactions. We found that the reaction $\gamma p \to p\eta$ can be described well with the inclusion of the well-established $S_{11}(1535)$, $S_{11}(1650)$, $D_{13}(1520)$, and $D_{13}(1700)$ resonances, in addition to the mesonic current. Consideration of other well-established resonances in the same mass region, including the spin-5/2 resonances, $D_{15}(1675)$ and $F_{15}(1680)$, does not further improve the results qualitatively. For the reaction $\pi^- p \to n\eta$, the $P_{13}(1720)$ resonance is found to be important for reproducing the structure observed in the differential cross section data. Our model also improves the description of the reaction $NN \to NN\eta$ to a large extent compared to the earlier results by Nakayama *et al.* [Phys. Rev. C **68**, 045201 (2003)]. Further improvement in the description of these reactions and the difficulty to uniquely determine the nucleon resonance parameters in the present type of analysis are discussed.

PACS numbers: 25.20.Lj, 13.60.Le, 13.75.Gx, 14.20.Gk

I. INTRODUCTION

One of the primary motivations for studying the production of mesons off nucleons is to investigate the structure and properties of nucleon resonances and, in the case of heavy-meson productions, to learn about hadron dynamics at short range. In particular, a clear understanding of the production mechanisms of mesons heavier than the pion still requires further theoretical and experimental investigation. Apart from pion production, the majority of theoretical investigations of meson-production processes are performed within phenomenological meson-exchange approaches. Such an approach forces us to correlate as many independent processes as possible within a single model if one wishes to extract meaningful physics information. Indeed, this is the basic motivation behind the coupled-channels approaches.

In this paper, we present the result of our investigation of η-meson production in both the photon- and hadron-induced reactions,

$$\begin{aligned} \gamma + N &\to N + \eta, \\ \pi + N &\to N + \eta, \\ N + N &\to N + N + \eta. \end{aligned} \tag{1}$$

More specifically, we perform a combined analysis of the reactions, $\gamma p \to p\eta$, $\pi^- p \to n\eta$, $pp \to pp\eta$, and $pn \to pn\eta$ based on an effective Lagrangian approach.

The amount of data available for η-meson production is now considerable. In particular, in photoproduction processes off protons, a new generation of high-precision data are now available, not only for total and differential cross sections in a wide range of energies starting from threshold [1] but also for beam and target asymmetries [2]. Taken in combination, these data sets offer better opportunities for investigating the properties of nucleon resonances. In particular, much more detailed studies than in the past are possible now for resonances that may perhaps couple strongly to $N\eta$ but only weakly to $N\pi$. In this respect, the recent data on the quasi-free $\gamma n \to n\eta$ process [3] have attracted much interest in η-production processes in connection to the possible existence of a narrow (crypto-exotic) baryon resonance with a mass near 1.68 GeV which is still under debate [4]. To date, the narrow bump structure in the $\gamma n \to n\eta$ reaction cross section was reported by several groups [5, 6]. The existence of a narrow baryon resonance near 1.68 GeV has been also suggested earlier by several authors [7].

There are a large number of theoretical investigations of η photoproduction, mostly from the early 1990s to the present [8] and, especially, off protons. Most of them focus on the role of nucleon resonances and the extraction of the corresponding resonance parameters, but a variety of issues have also been addressed, such as the $NN\eta$ coupling constant [9], the $U_A(1)$ anomaly [10], and the extended chiral symmetry [11]. Among the more recent calculations which analyze the recent high-precision data are those of Refs. [12–14]. The η-MAID approach [12] is an isobar model which includes, in addition to the t-channel vector-meson exchange or its Reggeized version,

*Electronic address: nakayama@uga.edu
†Electronic address: yoh@comp.tamu.edu
‡Electronic address: helmut.haberzettl@gwu.edu

a set of well-established spin-1/2, -3/2, and -5/2 resonances. This model has been applied to the analyses of data for photoproduction as well as for electroproduction of the η meson. The Bonn-Gatchina-Giessen group [13] has developed a model which has been employed in a combined partial wave analysis of the photoproduction data with $N\pi$, $N\eta$, ΛK, and ΣK final states. This model considers fourteen nucleon resonances and seven Delta resonances for achieving a reasonable overall agreement with the whole database considered in their analysis.[1] He, Saghai, and Li have analyzed the η-photoproduction reaction in a chiral constituent quark model [14] by considering all of the one- to four-star rated resonances listed in the Review of Particle Data Group (PDG) [15].

In hadronic reactions, a noticeable amount of data for $NN \to NN\eta$ has been accumulated [16–19]. Here we have pp and $p\eta$ invariant mass distributions and the analyzing power near threshold in addition to differential and total cross sections. The $NN \to NN\eta$ process is particularly relevant for studying the role of the $N\eta$ final-state interaction (FSI). Most of the existing calculations (see, e.g., Refs. [20, 21] and references therein; see also Ref. [22]) take into account the effects of the NN FSI in one way or another which is well-known to influence the energy dependence of the cross section near threshold. Calculations which include the $N\eta$ FSI to lowest order [23] reproduce the bulk of the energy dependence exhibited by the data. However, they are not sufficient to reproduce the pp invariant mass distribution measured by the COSY-TOF [17] and COSY-11 Collaborations [18]. Thus, in order to explain the observed pp invariant mass distribution, the importance of the three-body nature of the final state (in the S-wave) has been emphasized [24] or an extra energy dependence in the basic production amplitude has been suggested [25]. Yet, another possibility has been offered, which is based on the higher partial wave (P-wave) contribution [26]. We observe that what is actually required to reproduce the measured pp invariant mass distribution is an extra p'^2 dependence, where p' denotes the relative momentum of the final pp subsystem. Obviously, this can be achieved either by an S-wave or by a P-wave contribution. Note that the NN P-wave ($^3P_0$) can also yield a flat proton angular distribution as observed in the corresponding data. The model of Ref. [26], however, underpredicts the measured total cross near threshold to a large extent. One of the objectives of the present study is to resolve this discrepancy. In any case, as pointed out in Ref. [26], the measurement of the spin-correlation functions should help settle the question of the S-wave versus P-wave contributions in a model-independent way.

Most data for more basic (two-body) $\pi N \to N\eta$ reaction have been obtained in the 1960s through 1970s; they are rather scarce and less accurate [27] than for the other two reactions mentioned above. Recently, the Crystal Ball Collaboration has measured the differential and total cross sections of this reaction near threshold [28]. Theoretically, this reaction has been studied mostly in conjunction with other reactions in a combined analysis [29] or in coupled-channels approaches [30–34] in order to constrain some of the model parameters. Recently, Zhong *et al.* [35] have extended the chiral constituent quark model for meson photoproduction [14] to this reaction. Also, $\pi N \to N\eta$ has been studied within a heavy-baryon chiral perturbation theory [36]. Arndt *et al.* [37] have investigated the role of $\pi N \to N\eta$ on the $N\eta$ scattering length within a coupled-channels analysis of this reaction and the elastic πN scattering.

In the present work, we consider the three reactions mentioned above in the following manner: The photoproduction reaction is calculated by considering the s-, u- and t-channel Feynman diagrams plus a generalized contact term [38], which ensures gauge invariance of the total amplitude, in addition to accounting for the final-state interaction effects. (See Ref. [39] for details.) The $\pi N \to N\eta$ reaction is calculated in the tree-level approximation including the s-, u-, and t-channels. To the extent that this reaction is dominated by the excitation of the $S_{11}(1535)$ resonance at least for energies close to the threshold, this should be a reasonable approximation if we confine ourselves to energies not too far from the threshold. The $NN \to NN\eta$ process is calculated in the Distorted-Wave Born Approximation (DWBA), where both the NN FSI and the initial-state interaction (ISI) are taken into account explicitly [20]. The NN FSI is known to be responsible for the dominant energy dependence observed in the total cross section (apart from the dependence due to the phase space) arising from the very strong interaction in the S-wave states at very low energies [43]. As for the basic meson-production amplitude, our model includes the nucleonic, mesonic, and nucleon resonance currents which are derived from the relevant effective Lagrangians.

Ultimately, our goal is to perform a more complete model calculation where the relevant FSIs are taken into account explicitly. However, before being able to undertake a complex calculation that couples many channels, we need to learn some of the basic features of meson production (in particular, those of η-meson production) within a simplified model where these basic features may be revealed and analyzed in a much easier manner. In this regard, one of the major purposes of the present investigation is to show that consideration of the hadronic reactions $NN \to NNM$, in conjunction with more basic two-body reactions, would greatly help in the study of nucleon resonances, especially, in imposing much stricter constraints on the extracted resonance-nucleon-meson (RNM) coupling strength involving a meson M other than the pion. In fact, currently, our knowledge of the branching ratios of the majority of the known resonances is very limited [15].

[1] The Δ resonances do not coupled to the $N\eta$ and ΛK channels because of isospin conservation.

This paper is organized as follows. In the next section, we briefly describe our model for the reactions listed in Eq. (1). The results of the corresponding model calculations are presented and discussed in Sec. III. Section IV contains a summary and conclusion. Some details of the present model are given in the Appendix.

II. REACTION MECHANISMS

In the present work, the η-meson production processes are treated within a relativistic meson-exchange approach, whose dynamical contents are summarized by the Feynman diagrams displayed in Figs. 1, 2, and 3, for the reactions $\gamma N \to N\eta$, $\pi N \to N\eta$, and $NN \to NN\eta$, respectively. We employ phenomenological form factors at hadronic vertices to account for the structure of the corresponding hadrons.

For the photoproduction process, the total amplitude in the present work is given by the Feynman diagrams displayed in Fig. 1. Gauge invariance of the total amplitude is ensured by a generalized contact current given in Refs. [38, 39] that follows the general formalism of Refs. [40–42]. This contact term provides a rough phenomenological description of the FSI which is not treated explicitly here [39]. The details of the present approach are fully described in Ref. [38], where η'-meson production in photon- and hadron-induced reactions was investigated, and they will not be repeated here. One new feature in the present work, however, is the inclusion of spin-5/2 resonance contributions.

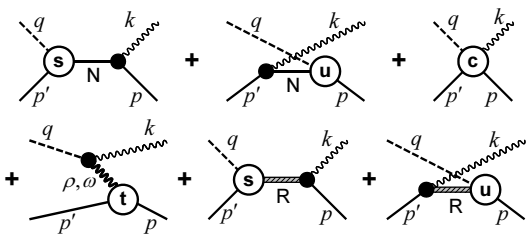

FIG. 1: Feynman diagrams contributing to $\gamma p \to p\eta$. Time proceeds from right to left. The wavy, solid, and dashed lines represent the photon, the nucleon, and the η meson, respectively. The intermediate baryon states are denoted by N and R for the nucleon and the nucleon resonances, respectively. The intermediate mesons in the t-channel include the ρ and ω. The external legs are labeled by the four-momenta of the respective particles and the labels s, u, and t of the hadronic vertices correspond to the off-shell Mandelstam variables of the respective intermediate particles. The three diagrams in the lower part are transverse individually; the three diagrams in the upper part are made gauge-invariant by the generalized contact current depicted in the top-right diagram. The nucleonic current (nuc) referred to in the text corresponds to the top line of diagrams; the meson-exchange current (mec) and resonance current contributions correspond, respectively, to the leftmost diagram and the two diagrams on the right of the bottom line of diagrams.

As mentioned in Sec. I, the reaction $\pi N \to N\eta$ is calculated within the tree-level approximation. To the extent that it is dominated by the $S_{11}(1535)$ resonance contribution, this is a reasonable approximation at least near threshold. The total amplitude for this reaction is, therefore, given by the Feynman diagrams displayed in Fig. 2.

As for the $NN \to NN\eta$ reaction, the total amplitude is calculated within the DWBA,

$$M = (T_f G_f + 1) J (1 + G_i T_i), \tag{2}$$

where $T_{i(f)}$ denote the NN ISI (FSI); $G_{i(f)}$ stands for the corresponding NN propagator; J denotes the basic production amplitude displayed in Fig. 3 and is constructed from the interaction Lagrangians given in the Appendix.

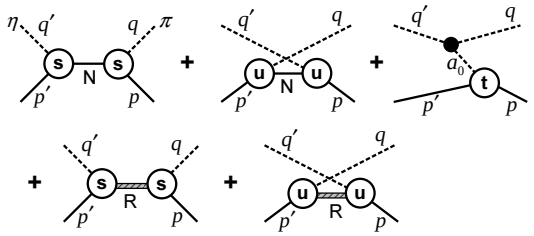

FIG. 2: Feynman diagrams contributing to $\pi^- p \to n\eta$. The notation is the same as in Fig. 1. The nucleonic current (nuc) referred to in the text corresponds to the first two diagrams on the top line; the meson-exchange current (mec) and resonance current contributions correspond, respectively, to the rightmost diagram on the top line and the two diagrams on the bottom line.

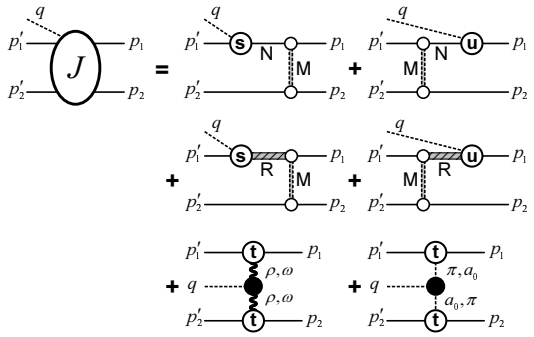

FIG. 3: Basic production amplitude for $NN \to NN\eta$. Time proceeds from right to left. As in Fig. 1, N and R denote the intermediate nucleon and resonances, respectively, and M incorporates all exchanges of mesons π, η, ρ, ω, σ, and a_0 (former δ) for the nucleon graphs and π, η, ρ, and ω for the resonance graphs. External legs are labeled by the four-momenta of the respective particles; the hadronic vertices s, u, and t correspond to the same kinematic situations, respectively, as those identified similarly in Fig. 1. The nucleonic, resonance, and meson-exchange contributions referred to in the text correspond, respectively, to the first, second, and third lines of the Feynman diagrams on the right-hand side. Diagrams with $p_1 \leftrightarrow p_2$ are not displayed but are included in the calculation. The full amplitude, including the NN ISI and FSI contributions, is given by Eq. (2).

Further details of the present approach to this reaction can be found in Ref. [20]. Also, we use the NN interaction based on the Paris potential [44], which includes the Coulomb interaction as well [45].

In the Appendix, we present all the hadronic and electromagnetic interaction Lagrangians and propagators necessary for computing the diagrams displayed in Figs. 1, 2, and 3 within the present approach. The phenomenological form factors used in this model are also given in the Appendix.

The free parameters of our model — the resonance parameters, the $NN\eta$ coupling constant, and the cut-off parameter Λ_v^* at the electromagnetic vector-meson exchange vertex — are fixed such as to reproduce the available data in a global fitting procedure of the three reaction processes listed in Eq. (1).

III. RESULTS AND DISCUSSION

In this section, we present and discuss the results of our model calculation. The basic strategy of our approach is in principle the same as that of Ref. [38], namely, we start with the nucleon plus meson-exchange currents and add resonance contributions one by one as needed in the fitting procedure until achieving a reasonable description of the available experimental data for the reactions listed in Eq. (1). Apart from the dominant $S_{11}(1535)$ resonance, we allow for other well-established resonances of spin-1/2, -3/2, and -5/2 in this model. We find that, in addition to spin-1/2 resonances, one needs at least spin-3/2 resonances — in particular, D_{13} resonances — in order to obtain a reasonable description of the data in the present approach.

Following Ref. [38], for each resonance we take into account only the branching ratios $\beta_{N\pi}$, $\beta_{N\eta}$, and $\beta_{N\pi\pi}$ corresponding to the respective hadronic decay channels $R \to N\pi$, $R \to N\eta$, and $R \to N\pi\pi$. The latter accounts *effectively* for all the other open decay channels. Note that the branching ratios $\beta_{N\pi}$ and $\beta_{N\eta}$ are related to the corresponding $RN\pi$ and $RN\eta$ coupling constants in the interaction Lagrangians and, as such, they are *not* free parameters of the model. The same is true for the branching ratio $\gamma_{N\gamma}$, associated with the radiative decay channel, which is related to the corresponding $RN\gamma$ coupling constants. Then, in view of the constraint given by Eq. (A.31), the branching ratio $\beta_{N\pi\pi}$ is not a free parameter, either. Here, we emphasize that, in contrast to Ref. [38] — where some assumptions were made concerning the values of the branching ratios $\beta_{N\pi}$ — no such assumptions are enforced in the present work since the simultaneous consideration of the reaction processes listed in Eq. (1) allows us, in principle, to extract the $RN\pi$ and $RN\eta$ coupling constants separately.

The coupling constants of the RNV ($V = \rho, \omega$) interaction Lagrangians are required in the calculation of the $NN \to NN\eta$ reaction. Therefore, in principle, one should also take into account the hadronic branching ratios involving vector mesons (such as the ρ and ω). However, since we have restricted ourselves to nucleon resonances for which the decay channels $R \to NV$ are either closed or nearly closed, we have set the associated branching ratios to zero ($\beta_{NV} = 0$).[2] In a test calculation, we found that this does not affect our conclusions. Obviously, in a more refined calculation, this condition should be relaxed. In a more complete (coupled-channels) dynamical model approach, the branching ratios and total widths will be generated by the model via the dressing mechanism of the corresponding vertices and resonance masses.

The results shown here are not necessarily of the best fit quality one can achieve within the present approach. Rather, they are sample fit results that illustrate different dynamical features one may obtain in this type of analysis. The resonance parameters are obtained by global fitting to the available data for the reactions mentioned above. In the following, we present and discuss the results for each reaction.

A. $\gamma p \to p\eta$

We first consider the model in which only the $S_{11}(1535)$, $S_{11}(1650)$, $D_{13}(1520)$, and $D_{13}(1700)$ resonance currents are considered in addition to the nucleonic and mesonic currents (cf. Fig. 1). We find that this comprises the minimal set of resonances that are required to achieve a reasonable description of the reaction processes listed in Eq. (1). The resulting fitted parameters are given in Table I, which are obtained by χ^2 fitting to the experimental data shown in Fig. 4 (however, not taking into account the total cross sections for $\gamma p \to p\eta$). Note that for photoproduction, in addition to the electromagnetic couplings, only the hadronic vertices involving the η meson are required for the present calculation. In the $\pi^- p \to n\eta$ reaction, only the hadronic vertices involving η and π are needed, while all the hadronic vertices given in the Appendix are required for the calculation of the $NN \to NN\eta$ reaction.

In Table I, the parameter values in boldface are fixed and are not allowed to vary during the fitting procedure. The pure pseudovector coupling choice ($\lambda = 0$) at the $NN\eta$ vertex was motivated by the massless chiral limit of the η meson. (See the Appendix for the definition of λ.) However, we will also consider the pseudoscalar coupling choice ($\lambda = 1$) in subsection III B. Also, the most general form of the RNV vertex for spin-3/2 and -5/2 resonances involves three independent coupling constants as exhibited in Eqs. (A.8) and (A.10). At present, however, information on the corresponding coupling constants are extremely scarce, especially, on $g^{(3)}_{RNV}$ defined

[2] Strictly speaking, even these resonances can have non-vanishing branching ratios to NV channels due to their large widths.

TABLE I: Model parameters fitted to the reactions listed in Eq. (1). (See the Appendix for explanation of the parameters.) Values in boldface are *not* fitted. The branching ratios $\gamma_{N\gamma}$ and β_{Nj} ($j = \pi, \eta, \pi\pi$) are not free parameters but are extracted from the corresponding coupling constants, except for $\beta_{N\pi\pi}$ which is obtained from Eq. (A.31). The values in square brackets are the range estimates quoted in PDG [15]. The data set for $\gamma p \to p\eta$, $\pi^- p \to n\eta$, and $NN \to NN\eta$ are used in the fit.

Nucleonic current:				
$(g_{NN\eta},\, \lambda)$	(0.007, **0.0**)			
Mesonic current:				
Λ_v^* (MeV)	1168			
N_{11} current:	$S_{11}(1535)$	PDG	$S_{11}(1650)$	PDG
M_R (MeV)	1540	[1525–1545]	1615	[1645–1670]
$g^{(1)}_{RN\gamma}$	0.81		0.52	
$(g_{RN\pi},\, \lambda)$	(−0.67, 0.04)		(−0.50, 0.77)	
$(g_{RN\eta},\, \lambda)$	(−2.61, 0.46)		(0.98, 0.91)	
$(g_{RN\omega}, f_{RN\omega})$	(38.52, −1.39)		(86.78, 6.19)	
$(g_{RN\rho}, f_{RN\rho})$	(−15.07, 2.67)		(−39.01, 10.84)	
Γ_R (MeV)	200	[125–175]	144	[145–185]
$\gamma_{N\gamma}$ (%)	0.31	[0.15–0.35]	0.24	[0.04–0.18]
$\beta_{N\pi}$ (%)	32	[35–55]	27	[60–95]
$\beta_{N\eta}$ (%)	65	[45–60]	19	[3–10]
$\beta_{N\pi\pi}$ (%)	2	[1–10]	54	[10–20]
N_{13} current:	$D_{13}(1520)$	PDG	$D_{13}(1700)$	PDG
M_R (MeV)	**1520**	[1515–1525]	**1700**	[1650–1750]
$(g^{(1)}_{RN\gamma}, g^{(2)}_{RN\gamma})$	(1.22, −0.18)		(0.21, −0.22)	
$g_{RN\pi}$	−1.96		0.58	
$g_{RN\eta}$	−3.32		−2.40	
$(g^{(1)}_{RN\omega}, g^{(2)}_{RN\omega}, g^{(3)}_{RN\omega})$	(−289.94, 242.59, **0.0**)		(341.79, −362.81, **0.0**)	
$(g^{(1)}_{RN\rho}, g^{(2)}_{RN\rho}, g^{(3)}_{RN\rho})$	(54.58, 154.53, **0.0**)		(−1.61, 90.18, **0.0**)	
Γ_R (MeV)	108	[100–125]	94	[50–150]
$\gamma_{N\gamma}$ (%)	0.41	[0.46–0.56]	0.07	[0.01–0.05]
$\beta_{N\pi}$ (%)	95	[55–65]	28	[5–15]
$\beta_{N\eta}$ (%)	0.03	$[0.23 \pm 0.04]$	2	$[0.0 \pm 1.0]$
$\beta_{N\pi\pi}$ (%)	5	[40–50]	70	[85–95]

in Eqs. (A.8) and (A.10). In the present work, therefore, we allow only two structures at those vertices by setting the coupling constant $g^{(3)}_{RNV}$ to zero.

In this work, we use the resonance masses from the centroid values quoted in PDG [15]. The exception to this is the masses of the $S_{11}(1535)$ and $S_{11}(1650)$ resonances. They were allowed to vary in the fitting process in order to reproduce the large cross-section peak exhibited by the photoproduction data near the threshold. The quantities in the square brackets in Table I are the range estimates quoted in PDG [15] and are given here for an easy comparison with the fitted values extracted in the present model. As one can see, some parameter values are considerably outside the range quoted in PDG. However, we note that, although various parameters are highly correlated to each other, the currently available data used in the present study are not sufficient to uniquely constrain the model parameters. As a result, different parameter sets may provide fits of comparable quality; some of them are discussed in this paper.

Figure 4 displays the results for photoproduction observables corresponding to the parameter set of Table I. The total cross section shown in Fig. 4(a) provides the line styles used in all four parts. We start with the discussion of the η angular distribution shown in Fig. 4(b). As one can see, the flat angular distribution near the threshold is dominated by the S_{11} resonance. When the photon incident energy (in the laboratory frame) T_γ is larger than about 1.0 GeV, both the D_{13} resonance and the mesonic currents become relevant for reproducing the shape of the measured differential cross sections. As energy increases, the shape becomes more and more forward-peaked, which is a well-known feature of the t-channel mesonic current contribution. In the energy region of $T_\gamma \approx 1.1$–2.0 GeV, some details of the measured angular distribution are still not well explained, which indicates that our model should be improved by a more refined and quantitative calculation. We leave such an investigation to a future work. The nucleonic current contribution is negligible because of very small coupling

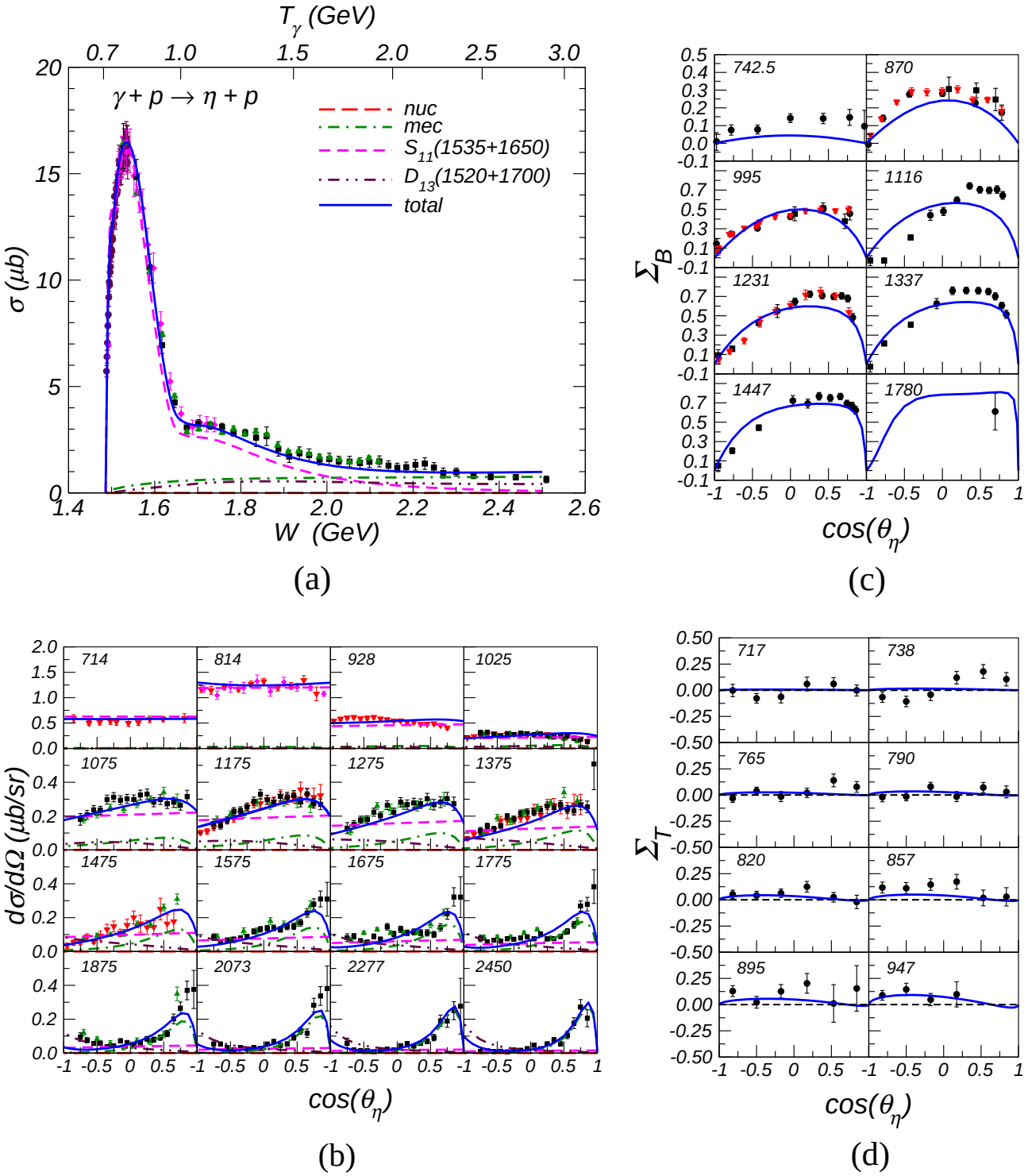

FIG. 4: (Color online) Results for the reaction $\gamma p \to p\eta$ employing the parameters of Table I. (a) Total cross section as a function of the total energy of the system W. The line styles identified here apply to all four parts of this figure. (b) η angular distribution in the center-of-mass frame. (c) Beam asymmetry Σ_B and (d) target asymmetry Σ_T in the center-of-mass frame. The numbers in (b,c,d) are the incident photon laboratory energies T_γ in MeV. In (c,d) only the total results are shown. The data are from Refs. [1, 2].

constant $g_{NN\eta}$ resulting from the fit, which is preferred by the small angular distribution measured at backward angles and higher energies. The nucleonic current contributes mostly at backward angles and at high energies

TABLE II: Another set of fitted parameters. See the caption of Table I for details.

Nucleonic current:				
$(g_{NN\eta},\, \lambda)$	(0.088, **0.0**)			
Mesonic current:				
Λ_v^* (MeV)	1202			
N_{11} current:	$S_{11}(1535)$	PDG	$S_{11}(1650)$	PDG
M_R (MeV)	1527	[1525–1545]	1625	[1645–1670]
$g^{(1)}_{RN\gamma}$	−0.55		0.38	
$(g_{RN\pi},\, \lambda)$	(0.43, 0.005)		(−0.37, 0.84)	
$(g_{RN\eta},\, \lambda)$	(1.92, 0.44)		(0.68, 0.86)	
$(g_{RN\omega}, f_{RN\omega})$	(−3.86, 0.79)		(8.81, −29.85)	
$(g_{RN\rho}, f_{RN\rho})$	(29.18, 8.40)		(4.09, 3.63)	
Γ_R (MeV)	99	[125–175]	162	[145–185]
$\gamma_{N\gamma}$ (%)	0.27	[0.15–0.35]	0.12	[0.04–0.18]
$\beta_{N\pi}$ (%)	26	[35–55]	13	[60–95]
$\beta_{N\eta}$ (%)	63	[45–60]	9	[3–10]
$\beta_{N\pi\pi}$ (%)	10	[1–10]	78	[10–20]
N_{13} current:	$D_{13}(1520)$	PDG	$D_{13}(1700)$	PDG
M_R (MeV)	**1520**	[1515–1525]	**1700**	[1650–1750]
$(g^{(1)}_{RN\gamma}, g^{(2)}_{RN\gamma})$	(−0.025, −2.51)		(0.59, −0.25)	
$g_{RN\pi}$	1.96		0.003	
$g_{RN\eta}$	2.81		−7.17	
$(g^{(1)}_{RN\omega}, g^{(2)}_{RN\omega}, g^{(3)}_{RN\omega})$	(−34.75, 2.91, **0.0**)		(−10.55, 14.65, **0.0**)	
$(g^{(1)}_{RN\rho}, g^{(2)}_{RN\rho}, g^{(3)}_{RN\rho})$	(−29.66, 24.37, **0.0**)		(−6.33, −2.39, **0.0**)	
Γ_R (MeV)	109	[100–125]	119	[50–150]
$\gamma_{N\gamma}$ (%)	0.70	[0.46–0.56]	0.24	[0.01–0.05]
$\beta_{N\pi}$ (%)	95	[55–65]	0.0006	[5–15]
$\beta_{N\eta}$ (%)	4	$[0.23 \pm 0.04]$	12	$[0.0 \pm 1.0]$
$\beta_{N\pi\pi}$ (%)	0.02	[40–50]	88	[85–95]

through the u-channel diagram (cf. Fig. 1). We will come back to this issue later in subsection III B.

Shown in Fig. 4(a) are the total cross section for η photoproduction obtained with the resonance parameters given in Table I. Here we mention that the total cross section data for photoproduction were *not* included in the global fitting process. As one can see, the large peak that rises sharply from threshold is due to the dominating $S_{11}(1535)$ and $S_{11}(1650)$ resonances. Although both the D_{13} resonance and mesonic currents are small, their contribution beyond $W \sim 1.6$ GeV cannot be ignored because of the interference with the large S_{11} current contribution. Around $W = 2.0$ GeV, all the resonance and mesonic currents become comparable to each other, but at higher energies, the mesonic current yields the largest contribution and the S_{11} resonance contribution becomes negligible as expected from their relative low mass. The structure shown by the data at $W \sim 2.2$ GeV seems to suggest possible contributions from other higher mass resonances. Analyses of this structure and other details are left to a future work.

Figure 4 also shows the results for the beam and target asymmetries. We find that, by and large, the beam asymmetry (Σ_B) and the target asymmetry (Σ_T) are described reasonably well.[3] The most visible room for improvement exists for the latter, in particular, at lower energies, where the data show a $\sin(2\theta_\eta)$ dependence while the model yields nearly flat and vanishing results. This is a feature common to all the parameter sets and not just to the particular parameter set of Table I. To understand the origin of this discrepancy, we consider the partial-wave contribution to the spin asymmetries. We expect that only a few partial waves contribute mostly to this reaction near the threshold. Then, considering only the S- and P-waves in the final state and following Ref. [47], the beam and target asymmetries are readily

[3] Quite recently, the GRAAL Collaboration [46] has re-analyzed the beam asymmetry in $\gamma p \to p\eta$ revealing a sharp structure at $W \sim 1.69$ GeV for $\theta_\eta \sim 43^\circ - 103^\circ$, suggesting the presence of a narrow resonance.

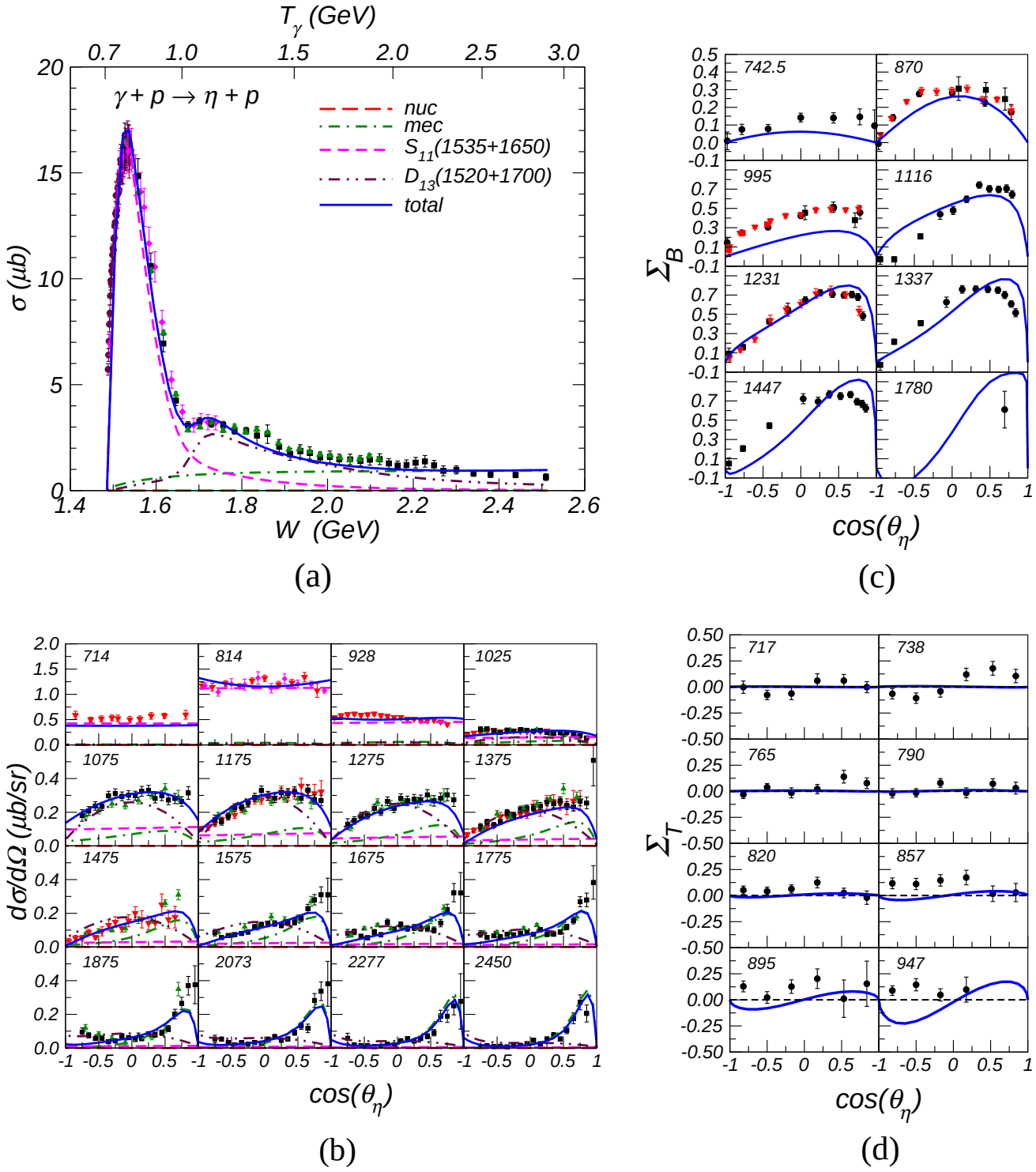

FIG. 5: (Color online) Same as Fig. 4 corresponding to the fitted parameter set of Table II.

given by

$$\frac{d\sigma}{d\Omega}\Sigma_B = \left(|\alpha_{L=1}|^2 - |\beta_{L=1}|^2\right)\sin^2(\theta_\eta),$$
$$\frac{d\sigma}{d\Omega}\Sigma_T = \mathrm{Im}\left[\delta^*_{L=0}\left(\beta_{L=1} - \alpha_{L=1}\right)\right]\sin(\theta_\eta) + \mathrm{Im}\left[\delta^*_{L=1}\left(\beta_{L=1} - \alpha_{L=1}\right)\right]\sin(2\theta_\eta), \quad (3)$$

which exhibits their respective angular dependence, where α_L, β_L, and δ_L stand for the linear combinations of the partial-wave matrix elements with the orbital angular momentum L in the final state. Then, it is easy to understand that it is more difficult to describe the latter observable because the beam asymmetry does not

TABLE III: Same as Table I. The $P_{13}(1720)$ resonance is added here to see whether it further improves the fit. No $NN \to NN\eta$ data were included in this fit.

Nucleonic current:						
$(g_{NN\eta}, \lambda)$	(0.003, **0.0**)					
Mesonic current:						
Λ_v^* (MeV)	1162					
N_{11} current:	$S_{11}(1535)$	PDG	$S_{11}(1650)$	PDG		
M_R (MeV)	1539	[1525–1545]	1617	[1645–1670]		
$g^{(1)}_{RN\gamma}$	1.01		0.58			
$(g_{RN\pi}, \lambda)$	(0.64, 0.008)		(0.42, 0.28)			
$(g_{RN\eta}, \lambda)$	(2.70, 0.36)		(−1.11, 0.62)			
Γ_R (MeV)	200	[125–175]	144	[145–185]		
$\gamma_{N\gamma}$ (%)	0.28	[0.15–0.35]	0.16	[0.04–0.18]		
$\beta_{N\pi}$ (%)	30	[35–55]	19	[60–95]		
$\beta_{N\eta}$ (%)	69	[45–60]	55	[3–10]		
$\beta_{N\pi\pi}$ (%)	0.72	[1–10]	25	[10–20]		
N_{13} current:	$D_{13}(1520)$	PDG	$D_{13}(1700)$	PDG	$P_{13}(1720)$	PDG
M_R (MeV)	**1520**	[1515–1525]	**1700**	[1650–1750]	**1720**	[1700–1750]
$(g^{(1)}_{RN\gamma}, g^{(2)}_{RN\gamma})$	(1.45, −0.14)		(0.01, 0.48)		(0.42, 1.44)	
$g_{RN\pi}$	−2.01		0.84		0.42	
$g_{RN\eta}$	−2.60		−2.64		0.74	
Γ_R (MeV)	114	[100–125]	126	[50–150]	192	[150–300]
$\gamma_{N\gamma}$ (%)	0.005	[0.46–0.56]	0.05	[0.01–0.05]	0.12	[0.003–0.01]
$\beta_{N\pi}$ (%)	95	[55–65]	44	[5–15]	95	[10–20]
$\beta_{N\eta}$ (%)	4	$[0.23 \pm 0.04]$	1.55	$[0.0 \pm 1.0]$	2.69	$[4.0 \pm 1.0]$
$\beta_{N\pi\pi}$ (%)	0.02	[40–50]	55	[85–95]	2.19	[> 70]

exhibit interference effects while the target asymmetry does. Equation (3) also shows that the S-wave final state does not contribute to the beam asymmetry.

Another parameter set resulting from the global fit, employing the same set of nucleon resonances as in Table I, is shown in Table II. This set was obtained by using different starting values for the search in parameter space during the fit procedure. As a result, many parameter values of this set are quite different from those of Table I not only in magnitude but also in relative signs for some coupling constants which provides an indication of the general reliability of such global fits. The corresponding observables are shown in Fig. 5. Here, although both the measured total and differential cross sections are reproduced with a comparable fit quality to the results in Fig. 4, the dynamical content is quite different. In particular, the $D_{13}(1700)$ resonance contribution dominates over the other currents in the energy region of $T_\gamma \approx 1.05$–1.5 GeV (i.e., $W \approx 1.7$–1.9 GeV). It is interesting to note that, searching for pole positions of the T-matrix in the complex plane as well as performing Breit–Wigner parameterizations of resonances, the recent partial-wave analysis by Arndt *et al.* [48] of $\pi^\pm p$ elastic and charge-exchange processes combined with the reaction $\pi^- p \to n\eta$ finds no $D_{13}(1700)$ resonance. Also, some of the coupled-channels dynamical models [32, 49] find no necessity for this resonance to fit the πN phase shifts. In this respect, the present results corresponding to the parameter set of Table I — where the contribution of the $D_{13}(1700)$ resonance is much smaller than that of Table II — are more in line with these findings. It would be most interesting to see if the inclusion of the γN channel in those coupled-channels analyses mentioned above will require the $D_{13}(1700)$ resonance. The spin observables in Fig. 5 exhibit overall the same features as in Fig. 4, but for higher energies the target asymmetry shows very different angular dependence for the two parameter sets which points to the importance of spin asymmetries in reducing the ambiguities that otherwise would exist.

Table III displays a parameter set including the $P_{13}(1720)$ resonance, in addition to those considered in the previous two sets. Here we have considered only the $\gamma p \to p\eta$ and $\pi^- p \to n\eta$ reaction data in the fitting procedure. The corresponding results for the observables are shown in Fig. 6. As can be seen, the inclusion of the $P_{13}(1720)$ resonance does not improve significantly the description of the data for this photon-induced reaction. However, as we will see in the following subsection, this resonance considerably improves the fit quality of the hadronic $\pi^- p \to n\eta$ reaction at higher energies.

Next, we extend our model by including all of the well-established resonances in the mass region of 1500 $\sim$

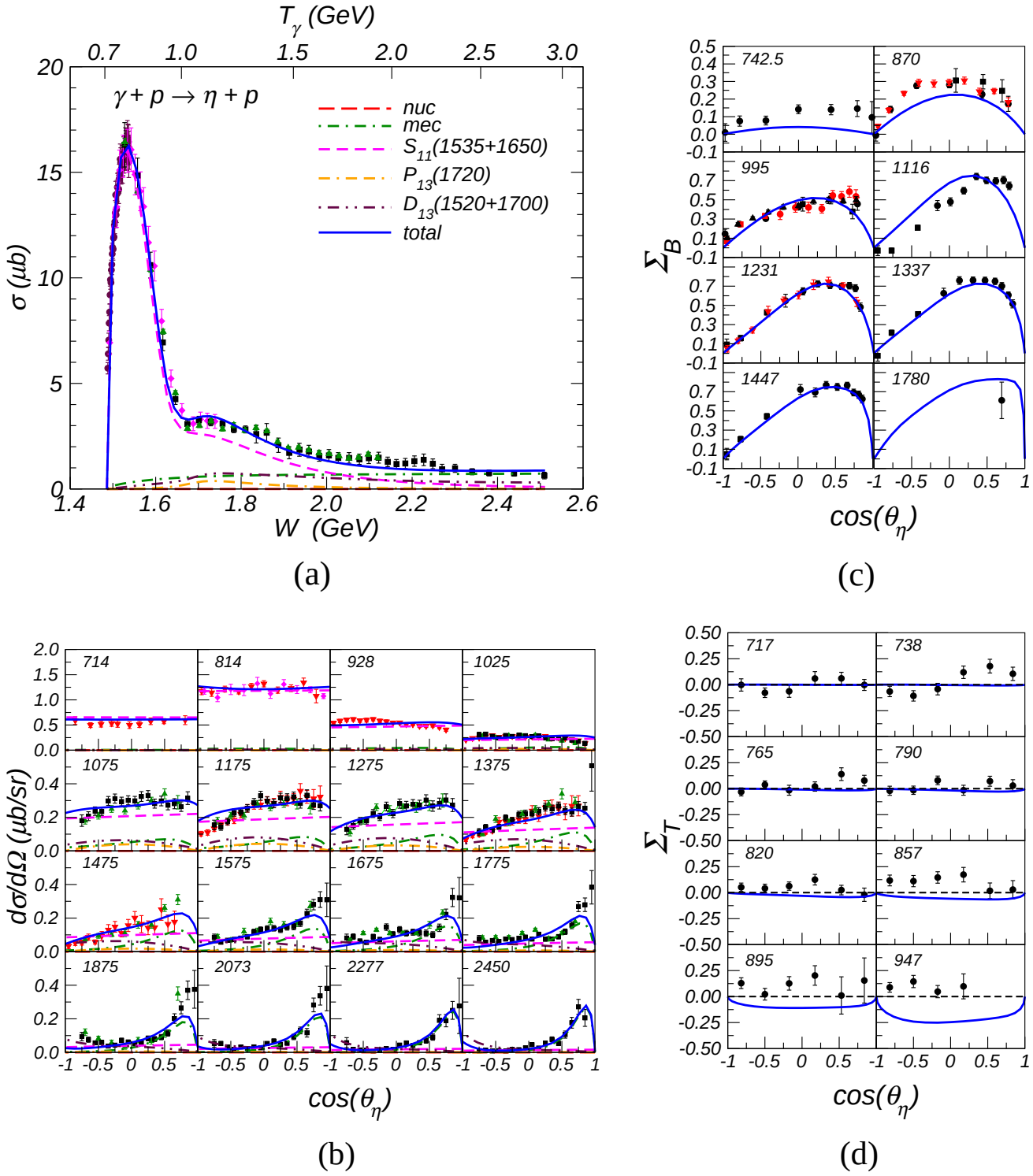

FIG. 6: (Color online) Same as Fig. 4 corresponding to the parameter set of Table III.

1700 MeV in order to verify whether these resonances can lead to a qualitatively superior description of the data compared to the previous cases, where a more limited set of resonances has been considered. To this end, we concentrate only on the $\gamma p \to p\eta$ reaction. Table IV shows the parameter set, where the $D_{15}(1675)$ and $F_{15}(1680)$ as well as the $P_{11}(1710)$ resonances are included, in addition to those considered in Table III. Here, following Ref. [38], we treat the branching ratio $\beta_{N\pi}$ as a free parameter to be fitted, while the branching ratio $\beta_{N\eta}$ is extracted from the product of the coupling constants $g_{RN\eta}g_{RN\gamma}$ in conjunction with the assumed branching ratio $\gamma_{N\gamma}$ for the

TABLE IV: Same as Table I. More resonances are added here to see whether they would further improve the fit. Here we have considered only the $\gamma p \to p\eta$ reaction in the fitting procedure.

Nucleonic current:						
$(g_{NN\eta}, \lambda)$	(0.07, **0.0**)					
Mesonic current:						
Λ_v^* (MeV)	1113					
N_{11} current:	$S_{11}(1535)$	PDG	$S_{11}(1650)$	PDG	$P_{11}(1710)$	PDG
M_R (MeV)	1521	[1525–1545]	1632	[1645–1670]	**1710**	[1680–1740]
$(g^{(1)}_{RN\gamma} g_{RN\eta}, \lambda)$	(1.22, 0.33)		(−0.49, 1.00)		(−0.63, 1.00)	
Γ_R (MeV)	110	[125–175]	174	[145–185]	250	[50–250]
$\gamma_{N\gamma}$ (%)	**0.26**	[0.15–0.35]	**0.06**	[0.04–0.18]	**0.01**	[0.002–0.05]
$\beta_{N\pi}$ (%)	30	[35–55]	18	[60–95]	81	[10–20]
$\beta_{N\eta}$ (%)	65	[45–60]	26	[3–10]	19	$[6.2 \pm 1.0]$
$\beta_{N\pi\pi}$ (%)	5	[1–10]	56	[10–20]	0.3	[40–90]
N_{13} current:	$P_{13}(1720)$	PDG	$D_{13}(1520)$	PDG	$D_{13}(1700)$	PDG
M_R (MeV)	**1720**	[1700–1750]	**1520**	[1515–1525]	**1700**	[1650–1750]
$g^{(1)}_{RN\gamma} g_{RN\eta}$	−0.85	0.22	0.37			
$g^{(2)}_{RN\gamma} g_{RN\eta}$	1.60	−10.32	−2.89			
Γ_R (MeV)	184	[150–300]	136	[100–125]	135	[50–150]
$\gamma_{N\gamma}$ (%)	**0.12**	[0.003–0.01]	**0.10**	[0.46–0.56]	**0.54**	[0.01–0.05]
$\beta_{N\pi}$ (%)	95	[10–20]	76	[55–65]	60	[5–15]
$\beta_{N\eta}$ (%)	5	$[4.0 \pm 1.0]$	0.04	$[0.23 \pm 0.04]$	4	$[0.0 \pm 1.0]$
$\beta_{N\pi\pi}$ (%)	0.04	$[> 70]$	24	[40–50]	36	[85–95]
N_{15} current:	$D_{15}(1675)$	PDG	$F_{15}(1680)$	PDG		
M_R (MeV)	**1675**	[1670–1680]	**1680**	[1680–1690]		
$g^{(1)}_{RN\gamma} g_{RN\eta}$	3.77		0.44			
$g^{(2)}_{RN\gamma} g_{RN\eta}$	14.12		−0.90			
Γ_R (MeV)	171	[130–165]	139	[120–140]		
$\gamma_{N\gamma}$ (%)	**0.02**	[0.004–0.022]	**0.25**	[0.21–0.32]		
$\beta_{N\pi}$ (%)	**45**	[35–45]	**65**	[65–70]		
$\beta_{N\eta}$ (%)	2	$[0.0 \pm 1.0]$	0.0001	$[0.0 \pm 1.0]$		
$\beta_{N\pi\pi}$ (%)	53	[50–60]	35	[30–40]		

radiative decay. The resulting observables with the parameter set of Table IV are shown in Fig. 7. We see that the overall fit quality does not change significantly from the previous sets. Here, the $D_{13}(1700)$ resonance gives the largest contribution to the cross section in the energy region of $W = 1.7$–2.0 GeV, a feature similar to what is exhibited already in Fig. 5.

B. $NN\eta$ coupling constant

In the previous subsection we have shown that the present calculations yield very small values of the coupling constant $g_{NN\eta}$ — compatible with zero — due to the smallness of the measured cross sections at backward angles where T_γ is large. As mentioned before, the η angular distribution becomes very sensitive to $g_{NN\eta}$ at these kinematics through the u-channel nucleonic current contribution. However, one must be cautious in drawing conclusions about the extracted value of $g_{NN\eta}$ from calculations based on approaches such as the present one. This is due to the fact that we cannot completely discard the possibility of a relatively large nucleonic current contribution interfering destructively with contributions from resonances in order to yield η angular distributions as observed at those kinematics. This point is illustrated in Fig. 8, where the results for η angular distribution are shown together with the data recently reported by Credé *et al.* (CB/ELSA Collaboration) [1] at the two highest energies. Figure 8(a) shows the results corresponding to the parameter set of Table IV, where the nucleonic current contribution is practically zero[4] and cannot be seen in the figure. The corresponding nucleon resonance contributions are also very small. The mesonic current

[4] Note that the value of $g_{NN\eta}$ is 0.07 in Table IV.

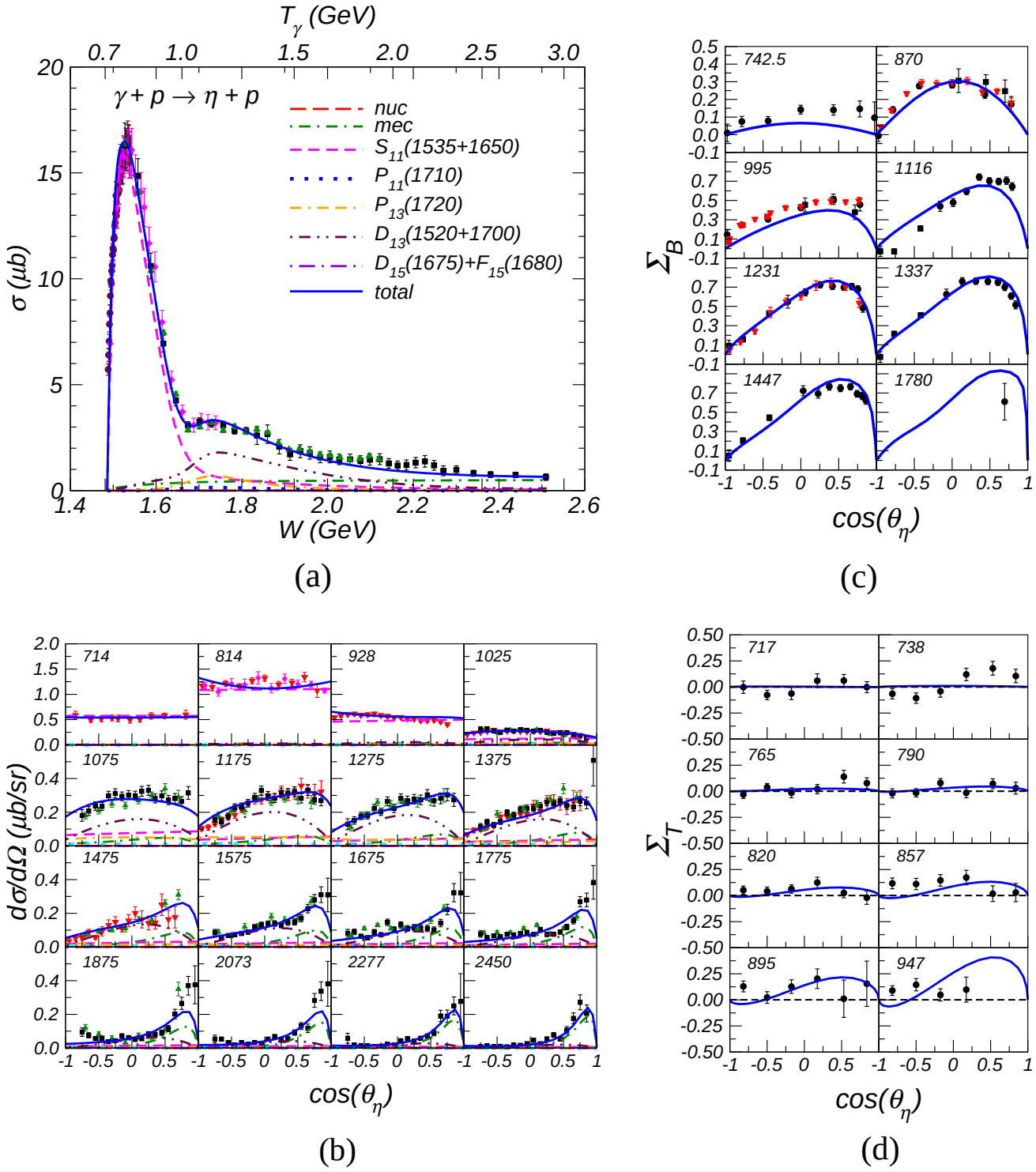

FIG. 7: (Color online) Same as Fig. 4 corresponding to the parameter set of Table IV.

dictates to a large extent the behavior of the angular distribution at forward angles. Figures 8(b,c) display the results corresponding to two additional parameter sets (not given here) with the same set of nucleon resonances as in Table IV. Overall, the two parameter sets yield a fit quality comparable to that of Fig. 7, but with very different resonance parameter values, which points to the ambiguity of the fit results if one relies solely on differential cross-section data. Shown in Fig. 8(b) is the result obtained by using pure pseudovector coupling ($\lambda = 0$) as in Fig. 7, while in Fig. 8(c) pure pseudoscalar coupling ($\lambda = 1$) is adopted. The corresponding $NN\eta$ cou-

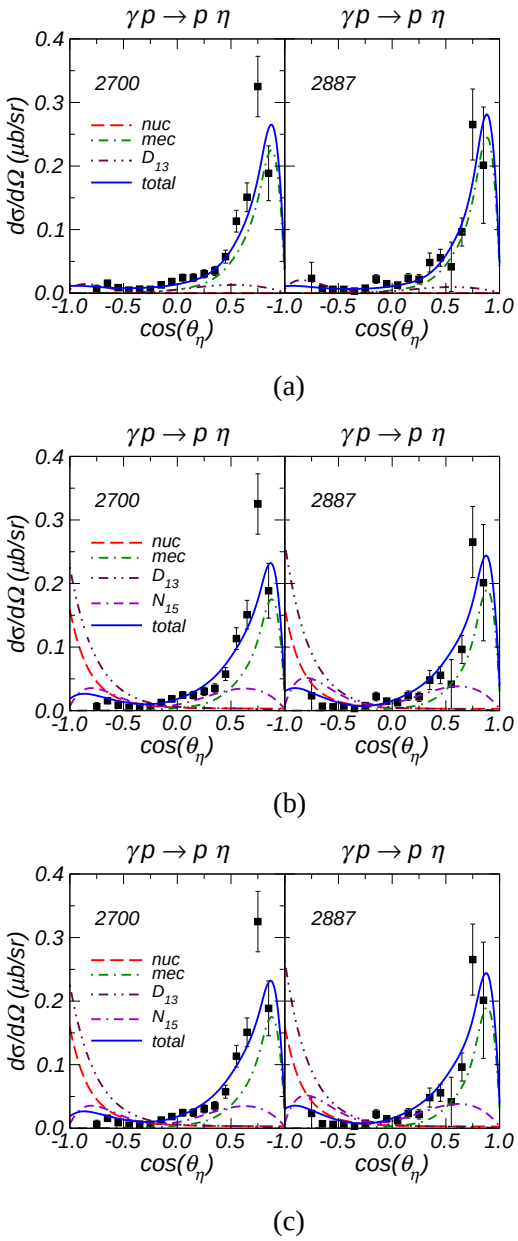

FIG. 8: (Color online) η-meson angular distributions in the center-of-mass frame in $\gamma p \to p\eta$ at $T_\gamma = 2700$ MeV and 2887 MeV. (a) The results corresponding to the parameter set of Table IV, with $g_{NN\eta} = 0.07$. (b,c) The results obtained with two other parameter sets (not given in this work) using the pseudovector ($\lambda = 0$) and pseudoscalar ($\lambda = 1$) coupling choices, respectively, at the $NN\eta$ vertex. The resulting $NN\eta$ coupling constant values are $g_{NN\eta} = 1.62$ and 1.38, respectively. The contributions from the other nucleon resonances are practically negligible at these energies and are not displayed. N_{15} is the sum of spin-5/2 resonance contributions. The data are from Credé *et al.* [1].

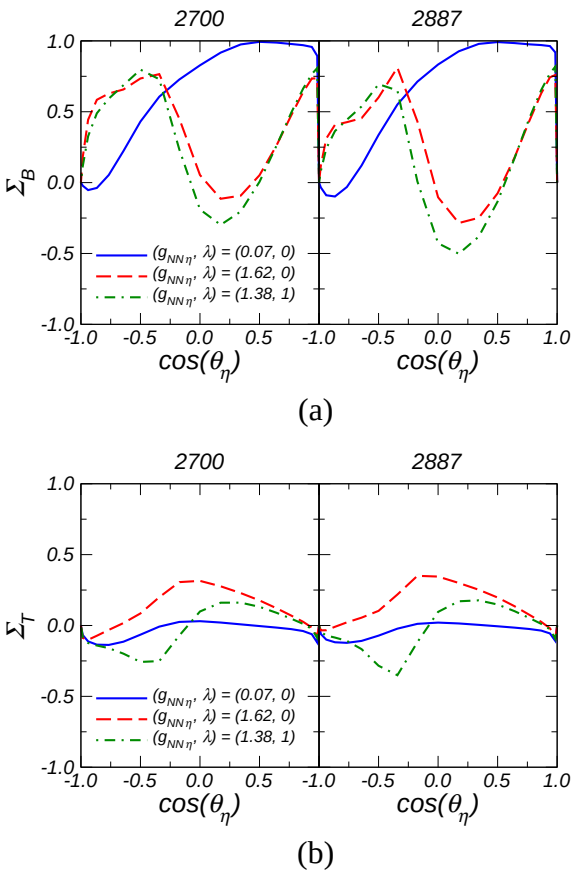

FIG. 9: (Color online) (a) Beam asymmetry Σ_B and (b) target asymmetry Σ_T in $\gamma p \to p\eta$ at $T_\gamma = 2700$ MeV and 2887 MeV as a function of η-emission angle in the center-of-mass frame. The solid curves represent the results obtained with the parameter set of Table IV, which correspond to Fig. 8(a). The dashed and dash-dotted curves are obtained with the two other parameter sets that correspond to Figs. 8(b) and (c), respectively.

pling constants are $g_{NN\eta} = 1.62$ and 1.38, respectively. As can be seen in Figs. 8(b,c), in these cases the nucleonic current contribution at backward angles is as large as that of the mesonic current at forward angles. However, the D_{13} resonance contribution exhibits a similar angular dependence as the nucleonic current with a comparable magnitude and interferes *destructively* with the nucleonic current. The destructive interference is almost complete and results in very small cross sections at backward angles as observed in the data. Overall, everything else being very similar between Figs. 8(b,c), we find no real sensitivity of the differential cross sections at these energies as to whether one employs pseudovector or pseudoscalar couplings.

The situation changes when one considers spin observables. While there is no real difference at lower energies, however, at the high energies ($T_\gamma = 2700 \sim 2887$ MeV) considered here, the beam asymmetry Σ_B shown in Fig. 9(a) can distinguish clearly between the parameter sets corresponding to Fig. 8(a) on the one hand and Figs. 8(b,c) on the other. The marked differences are due to the marked differences in the values for the $NN\eta$ coupling constant $g_{NN\eta}$, which is vanishingly small

($g_{NN\eta} = 0.07$) for the set corresponding to Fig. 8(a) and much larger (and about the same, $g_{NN\eta} = 1.62$ and $g_{NN\eta} = 1.38$, respectively) for Figs. 8(b) and (c). This finding shows that the beam asymmetry at higher energies can impose more stringent constraints, in particular, on the $NN\eta$ coupling constant. In any case, judging from the results in the present investigation, we expect the upper limit of the $NN\eta$ coupling constant to be not much larger than $g_{NN\eta} \approx 1.7$.

These parameter sets also lead to noticeable differences — albeit not quite as large — for the target asymmetry Σ_T, as shown in Fig. 9(b). Of particular importance, however, is that this observable can clearly distinguish between whether one employs pseudoscalar or pseudovector coupling at the $NN\eta$ vertex which the results of Figs. 8(b,c) and the respective curves of Fig. 9(a) cannot do.

Before closing this subsection, we remark that, quite recently, the authors of Ref. [11] have addressed the issue of chiral symmetry in η-meson photoproduction through the pseudoscalar-pseudovector mixing parameter λ at the $NN\eta$ vertex by investigating this reaction close to the threshold. Our study reveals that one must be careful with such an investigation for the reasons mentioned above. In particular, if the $NN\eta$ coupling constant turns out to be very small, it will be very difficult to determine the value of the mixing parameter λ.

C. $\pi^- p \to n\eta$

In this subsection, we discuss the $\pi^- p \to n\eta$ reaction with the parameter sets determined above. The results for the total and differential cross sections for the reaction $\pi^- p \to n\eta$ corresponding to the parameter sets of Tables I and II are displayed in Figs. 10(a,b) and Figs. 10(c,d), respectively. The cross-section results show that the various dynamical contributions of the two sets are very similar. The total cross section is rather well reproduced up to $W \approx 1.6$ GeV, where it is dominated by the S_{11} resonances, especially, by the $S_{11}(1535)$ resonance. Here, both the nucleonic and mesonic currents yield very small contributions. However, we do not reproduce the total cross section at higher energies due to the absence of the higher-mass resonances in these parameter sets and the absence of the $N\pi\pi$ contribution via the coupled channel [30, 32] in this model. For differential cross sections, we again note that these parameter sets are unable to reproduce the structure exhibited by the data at higher energies.

As we have shown before, the inclusion of the $P_{13}(1720)$ does not improve the results for the $\gamma p \to p\eta$ reaction significantly. However, this resonance provides an important contribution to reproduce the structure exhibited by the differential cross section data in $\pi^- p \to n\eta$. This is illustrated in Fig. 11 corresponding to the parameter set of Table III. In addition, the $P_{13}(1720)$ resonance also helps improve to some extent the fit quality for the total cross section above $W \approx 1.6$ GeV.

Figure 12 shows an alternative fit for the total and differential cross section using the same set of resonances as those of Fig. 11 plus $P_{11}(1710)$. The corresponding fit results for photoproduction are of comparable quality to those shown in Sec. III A. As one can see from Fig. 12(a), the small bump near $W = 1.7$ GeV in the spin-1/2 resonance contribution (dashed line) is caused by the $P_{11}(1710)$ resonance which makes the bump in the total contribution (solid line) more pronounced compared to the result of Fig. 11(a). The $P_{11}(1710)$ resonance seems also to affect the differential cross section in the vicinity of $W = 1670$ MeV, improving the agreement with the data to some extent. It is interesting to note that the recent chiral constituent quark-model calculation of Ref. [35] shows a dominant contribution from the $P_{11}(1710)$ resonance around $W = 1700$ MeV, in contrast to the present approach, where the dominant contribution arises from the spin-3/2 resonances. However, the authors of Ref. [35] have also found that the agreement with the measured differential cross sections in the $W = 1609$–1670 MeV energy range can be improved if the sign of their $P_{11}(1710)$ partial wave amplitude is reversed and if they employ a larger total decay width of $\Gamma_R \sim 350$ MeV. The effect of the $P_{11}(1710)$ resonance is, then, very similar to that found in the present calculation. We note that the total decay width of the $P_{11}(1710)$ resonance in Fig. 12 is $\Gamma_R = 95$ MeV.

D. $NN \to NN\eta$

In this subsection, we turn our attention to the $NN \to NN\eta$ reaction. Although the model calculation of Ref. [26], which is based on a strong P-wave contribution, reproduces nicely the shape of the measured pp invariant mass distributions, it largely underestimates the total cross section data near the threshold. Here we present new results based on a combined analysis of the reactions listed in Eq. (1).

Shown in Fig. 13 are the results for the $NN \to NN\eta$ reaction corresponding to the parameter set of Table I. It can be seen that the present model reproduces rather reasonably all the considered data for this reaction, including the energy dependence of the total cross sections at lower energies. This is a considerable improvement over the results of Ref. [26]. However, we still underestimate the total cross section in pp collisions by a factor of ~ 1.5 when the excess energy Q is $Q \leq 10$ MeV. We expect that the inclusion of $p\eta$ FSI and possibly the three-body effects would resolve this discrepancy once they are properly taken into account. Here, the major difference of our results from the previous calculation of Ref. [26] is that we have a much stronger spin-3/2 resonance contribution to the cross sections, especially at lower energies. This is due to the large coupling of the D_{13} resonances to the ρ and ω vector mesons, resulting from the global fitting procedure (cf. Table I). In contrast, the

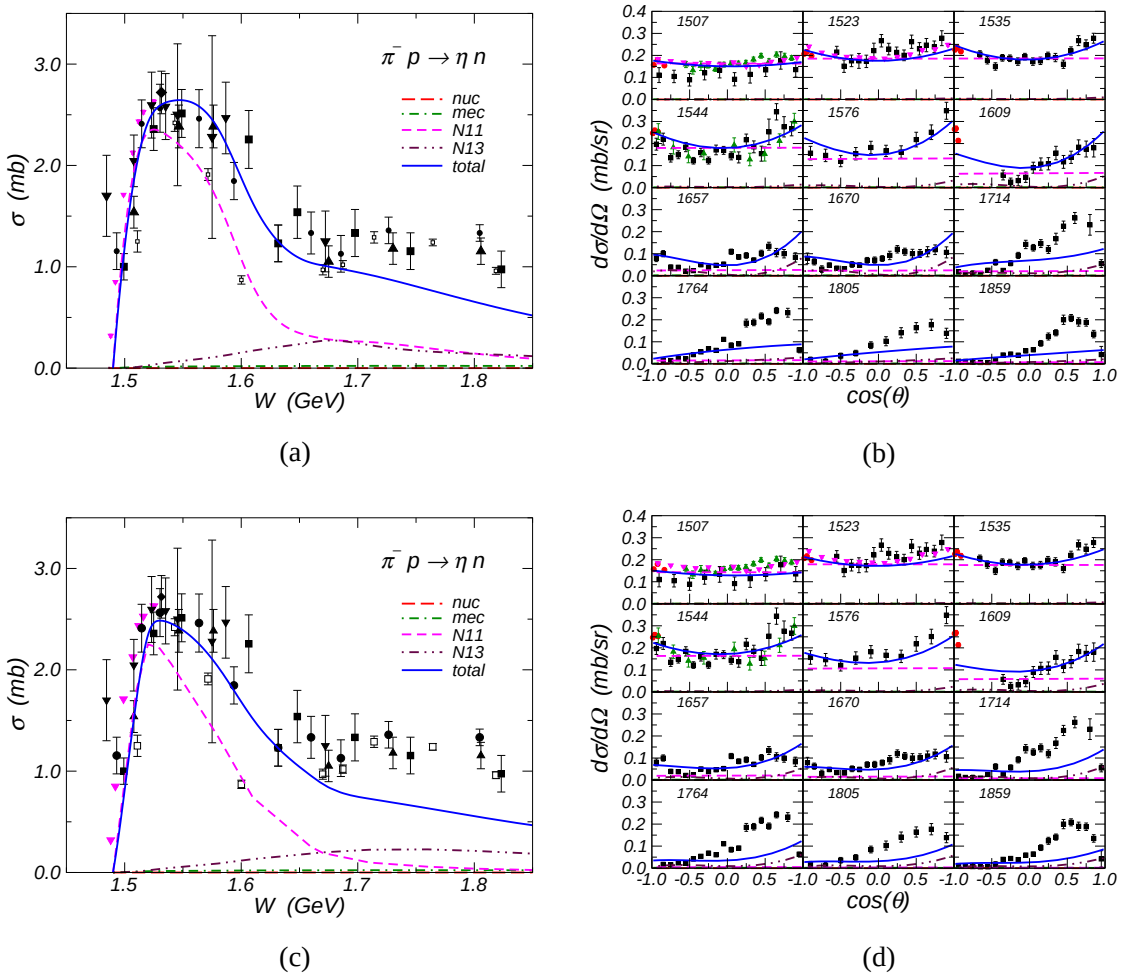

FIG. 10: (Color online) Results for $\pi^- p \to n\eta$ corresponding to the parameter set of Table I. (a) Total cross section as a function of the total energy of the system W. (b) η angular distribution in the center-of-mass frame. Here, $N11$ stands for $S_{11}(1535) + S_{11}(1650)$ contributions and $N13 = D_{13}(1520) + D_{13}(1700)$ contributions. (c,d) Same as (a) and (b) but with the parameter set of Table II. The numbers in (b) and (d) denote the total center-of-mass energy W in MeV. The labeling of the curves in (b,d) is the same to that of (a,c). The experimental data are from Ref. [27, 28].

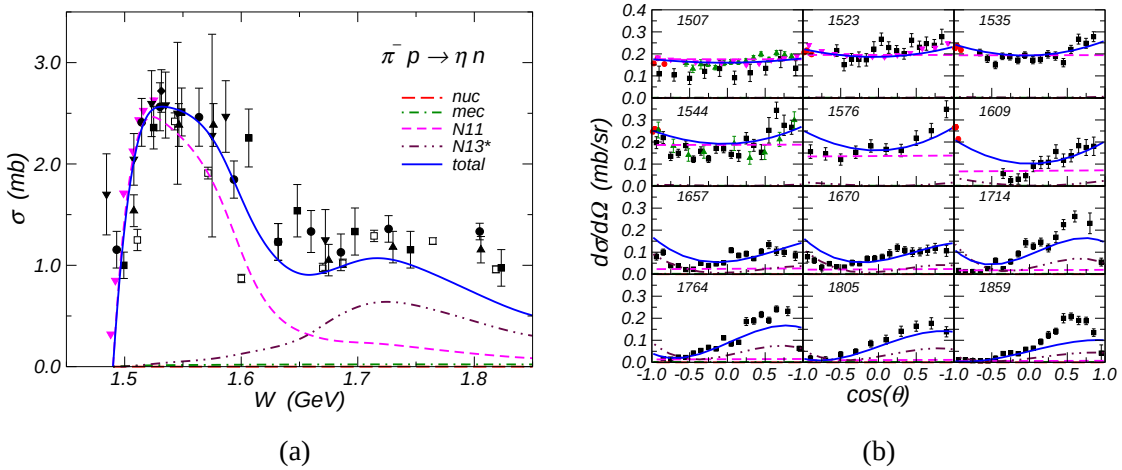

FIG. 11: (Color online) Same as Fig. 10 but corresponding to the parameter set shown in Table III. Here, $N13^* = D_{13}(1520) + D_{13}(1700) + P_{13}(1720)$.

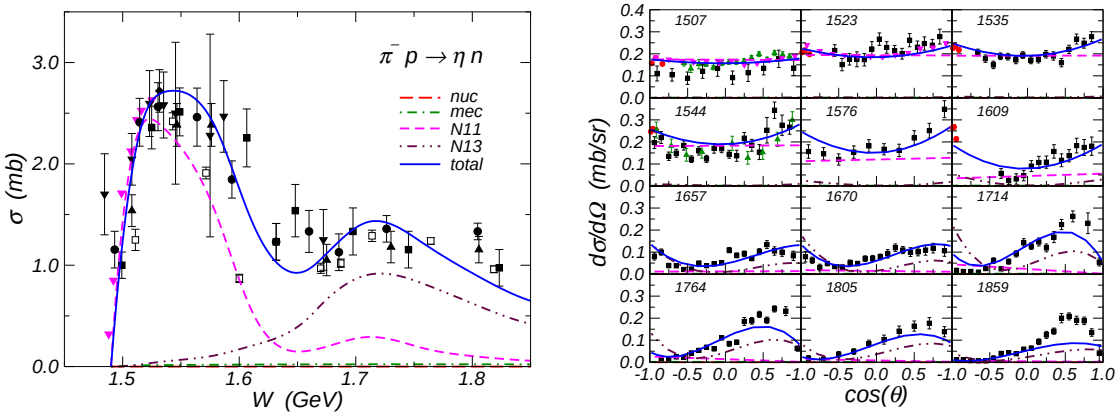

(a) (b)

FIG. 12: (Color online) Same as Fig. 11 but corresponding to another parameter set (not given here) that includes the $P_{11}(1710)$ resonance. Here, $N11 = S_{11}(1535) + S_{11}(1650) + P_{11}(1710)$.

S_{11} resonance contribution to the cross section is surprisingly small, especially at lower energies, which is due to the strong destructive interference among the exchanged mesons in the excitation of S_{11} resonances. Note that in the present calculation the resonance coupling constants involving vector mesons, g_{RNV} $(V = \rho, \omega)$, are basically fixed by the $NN \to NN\eta$ reaction, while the coupling constants to pseudoscalar mesons, g_{RNP} $(P = \pi, \eta)$, are fixed by the $\gamma p \to p\eta$ and $\pi^- p \to n\eta$ reactions to a large extent. We also found that the mesonic current yields a very small contribution to the cross sections. The nucleonic current contribution is also negligible because of the very small $NN\eta$ coupling constant that results from the fit to the photoproduction data, as discussed above.

It should be emphasized that it still remains to be verified whether the dominance of the D_{13} resonances discussed above is indeed true. In fact, in spite of the present lack of information on the corresponding coupling constants, $g^{(1,2)}_{RNV}$, the obtained values (cf. Table I) may be too large to be realistic. For example, a rough estimate of these coupling constants from the PDG helicity amplitudes [15] in conjunction with vector-meson dominance yields

$$\text{for } R = D_{13}(1520): \quad g^{(1)}_{RN\omega} \sim -57.3, \quad g^{(2)}_{RN\omega} \sim 82.3, \quad g^{(1)}_{RN\rho} \sim -23.9, \quad g^{(2)}_{RN\rho} \sim 19.0, \tag{4}$$

and

$$\text{for } R = D_{13}(1700): \quad g^{(1)}_{RN\omega} \sim -6.4, \quad g^{(2)}_{RN\omega} \sim 9.6, \quad g^{(1)}_{RN\rho} \sim -2.1, \quad g^{(2)}_{RN\rho} \sim 3.0. \tag{5}$$

These values are corrected to the normalization point, at $q^2 = M_V^2$, i.e., by writing

$$g^{(i)}_{RNV} \equiv \Gamma^{(i)}_{RNV}(p'^2 = M_R^2, p^2 = M_N^2, q^2 = M_V^2) = \frac{\Gamma^{(i)}_{RNV}(p'^2 = M_R^2, p^2 = M_N^2, q^2 = 0)}{F(p'^2 = M_R^2, p^2 = M_N^2, q^2 = 0)}, \tag{6}$$

where $\Gamma^{(i)}_{RNV}$ is the effective hadronic coupling function that includes the form factor F given by Eq. (A.17). We emphasize in this context that these coupling constants cannot be determined uniquely in the present analysis. Indeed, as shown in Fig. 14, a scenario in which the S_{11} resonance dominates over the D_{13} resonance current can be achieved. Therefore, the consistency of these coupling constant values with other independent reaction processes should be examined in detail. For this purpose, vector-meson production processes, such as $NN \to NNV$, $\pi N \to NV$ and $\gamma N \to NV$, are of particular interest [50].

In Ref. [20], where the dominant η-production mechanism is the excitation of the $S_{11}(1535)$ resonance via the pion-exchange, the analyzing power A_y exhibits a zero at $\cos(\theta_\eta) \sim 0$. In the present calculation, where the dominant production mechanism is the D_{13} resonance excitation, the zero of A_y is shifted toward backward angles at larger Q. As has been pointed out in Ref. [20], unlike the total and differential cross sections, the analyzing power is very sensitive to the reaction dynamics. In fact, the dashed curves in Fig. 13 for A_y represent the results of another parameter set (not given here) which yields practically the same results for other observables considered here (see also the results shown in Fig. 14 below). Unfortunately, the data are not accurate enough to disentangle these different scenarios. More accurate data will, therefore, impose more stringent constraints so as to help distinguish different dynamics of η production in NN collisions.

The results corresponding to the parameter set of Table II are shown in Fig. 14. They are of comparable

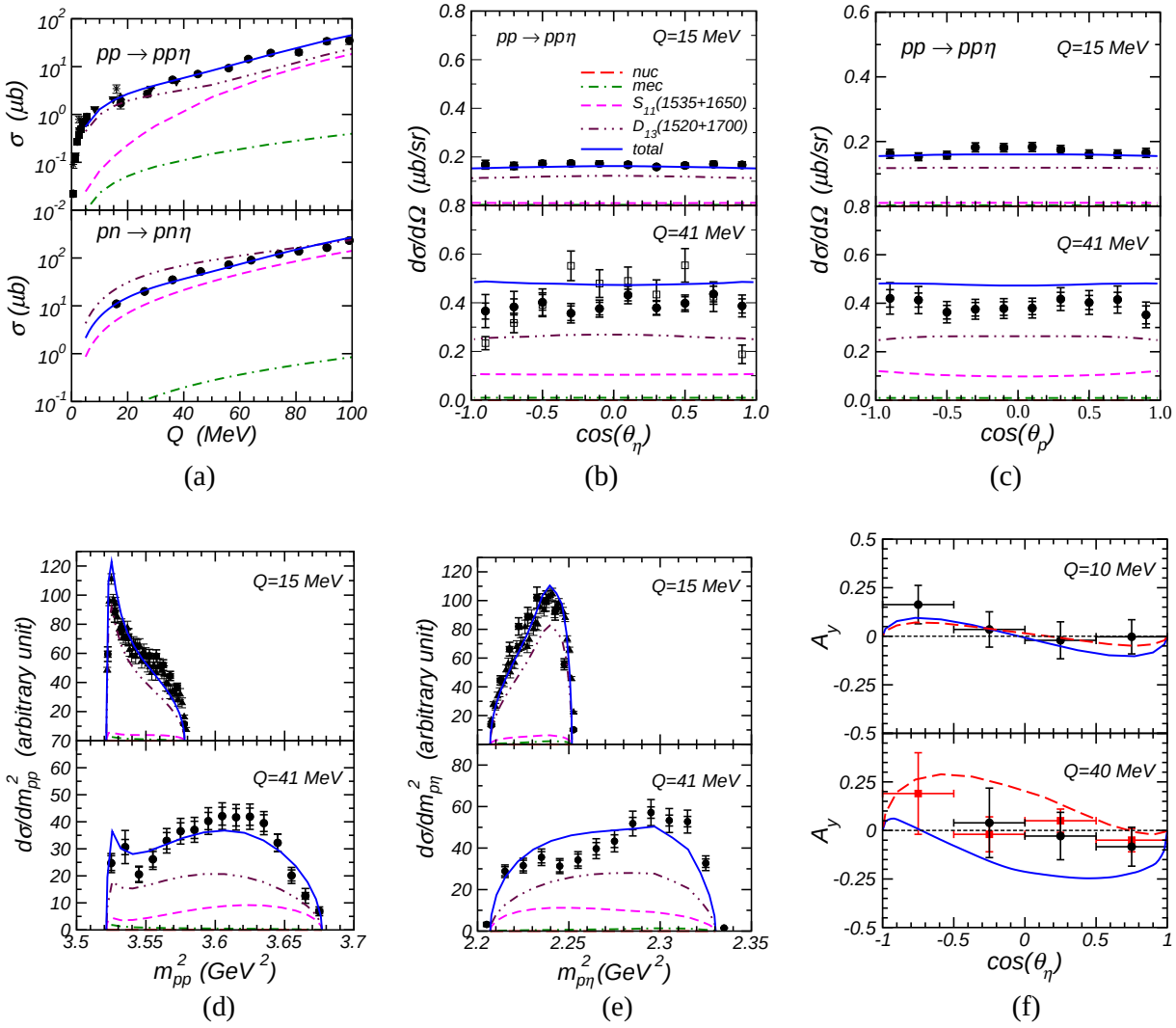

FIG. 13: (Color online) Results for the reaction $NN \to NN\eta$ corresponding to the parameter set of Table I. (a) Total cross section as functions of the excess energy Q in pp and pn collisions. (b) η angular distribution in the overall center-of-mass frame. (c) Final proton angular distribution. (d) pp invariant-mass distribution. (e) $p\eta$ invariant-mass distribution. (f) Analyzing power. In (f), only the total contributions are shown (solid curves); the dashed curves represent the correspond results of another parameter set (not given in this work) which yields practically the same results for other observables considered in this reaction. The labeling of the curves in (b,c,d,e) is the same as that in (a). The data are from Refs. [16–19].

fit quality to those in Fig. 13 overall. However, the dynamical content is quite different. In this case, the S_{11} resonance dominates over the D_{13} resonance contributions to the cross sections. Unlike the results shown in Fig. 13, there is no strong destructive interference among the exchanged meson contributions to excite the intermediate S_{11} resonances. Of course, the smallness of the D_{13} resonance contributions is directly correlated to the very small constants for the coupling of the D_{13} resonances to vector mesons (cf. Table II). The analyzing power for this parameter set at $Q = 40$ MeV exhibits a qualitatively different behavior from that found in Fig. 13. But again, the quality of the current experimental data does not allow to draw any definite conclusion.

It should be emphasized that the much larger difference in the dynamics in $NN \to NN\eta$ between the two parameter sets considered above as compared to those in $\gamma p \to p\eta$ and $\pi^- p \to n\eta$ stems from the much richer interference effects in the former reaction. In particular, note that, for each meson M exchanged $(\pi, \eta, \rho, \omega)$, there are two coupling vertices involved in the nucleon resonance currents (i.e., RNM and NNM, see Fig. 3). This allows for an interference among all the exchange mesons involving the RNM coupling constants, a feature that is absent in the other two reactions. Therefore, the meson-production reactions in NN collisions, in conjunction with other basic photon- and (two-body) hadron-induced reactions, should help in extracting the resonance parameters to a large extent. In particular, adding the vector meson (V) production channels, $NN \to NNV$,

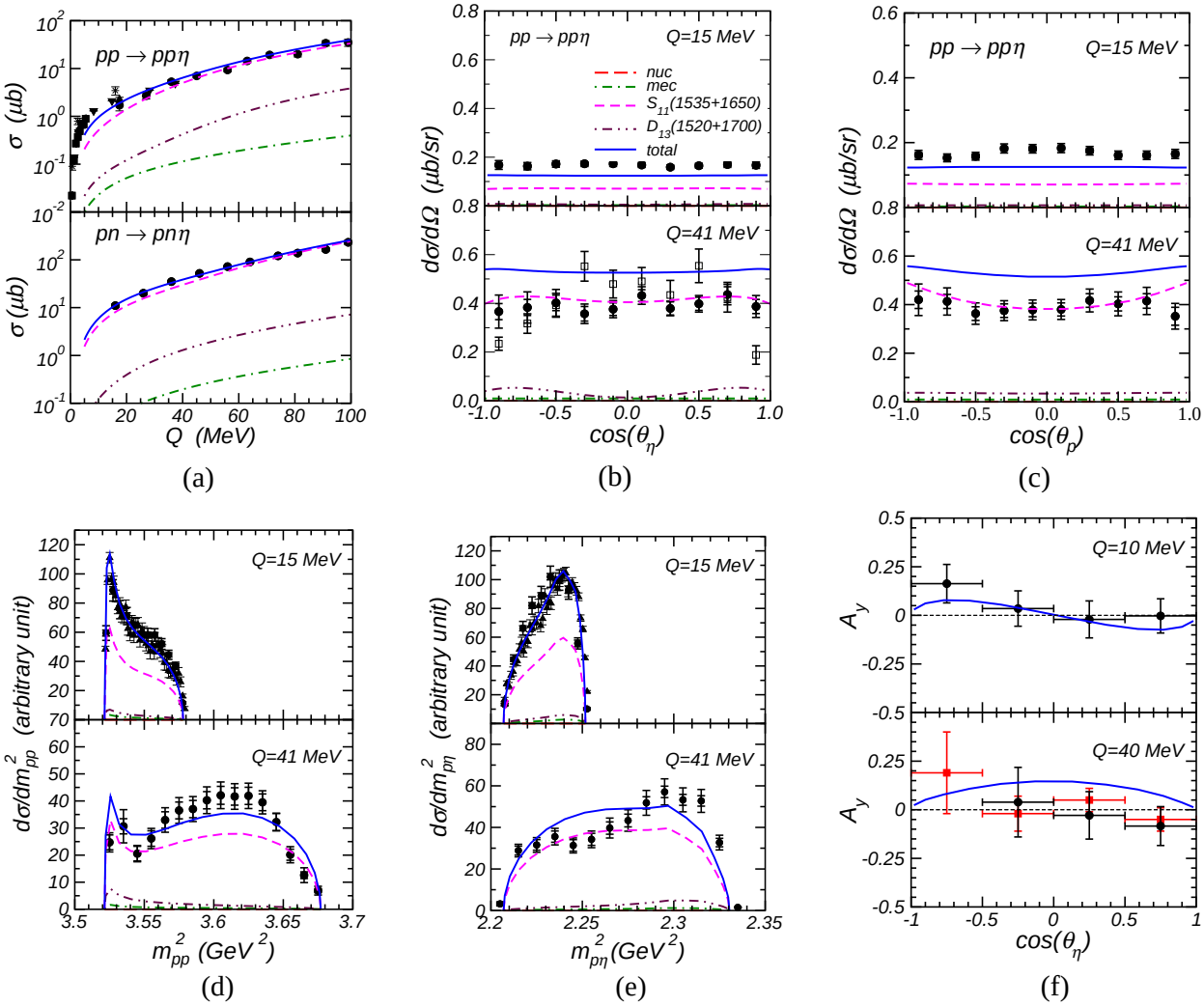

FIG. 14: (Color online) Same as Fig. 13 for the parameter set of Table II.

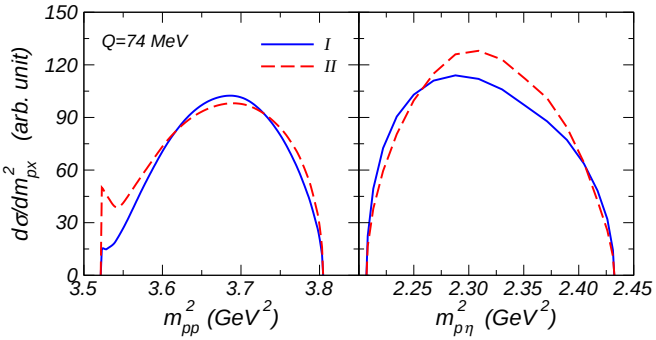

FIG. 15: (Color online) Predictions for the invariant-mass distributions $d\sigma/dm^2_{px}$ for pp ($x = p$) and $p\eta$ ($x = \eta$) in the reaction $pp \to pp\eta$ corresponding to the excess energy of $Q = 74$ MeV for the parameter sets of Tables I (solid line) and II (dashed line).

$\pi N \to NV$ and $\gamma N \to NV$, to the list of reactions given in Eq. (1), should impose more stringent constraints on the resonance coupling constants.

Finally, Fig. 15 shows predictions using the parameter sets of Tables I and II for the invariant-mass distributions for pp and $p\eta$ at the excess energy of $Q = 74$ MeV. At this energy, data have been measured at CELSIUS with the WASA detector [51].

IV. SUMMARY

In the present work, a combined analysis of the reactions $\gamma p \to p\eta$, $\pi^- p \to n\eta$, $pp \to pp\eta$, and $pn \to pn\eta$ has been carried out within a relativistic meson-exchange model of hadronic interactions. Both $\gamma p \to p\eta$ and $\pi^- p \to n\eta$ reactions have been treated in the tree-level approximation with the former reaction containing a generalized contact current which ensures gauge invariance of the reaction amplitude. The $NN \to NN\eta$ reaction has been treated in the DWBA approximation with the explicit treatment of the NN ISI and FSI. The free pa-

rameters of the model, especially the nucleon resonance parameters, are then fixed in a global fitting procedure.

Overall, the photoproduction data can be described reasonably well with the inclusion of the well-established $S_{11}(1535)$, $S_{11}(1650)$, $D_{13}(1520)$, and $D_{13}(1700)$ resonances as the minimally required set of resonances to achieve a reasonable fit to the currently available data. The inclusion of additional well-known resonances in the same mass region [including the spin-5/2 $D_{15}(1675)$ and $F_{15}(1680)$ resonances] does not further improve the quality of the overall description of the data. The measured angular distributions at higher energies and backward angles are compatible with a vanishing $NN\eta$ coupling constant. However, in order to extract this coupling constant unambiguously within an approach of the type pursued here, one needs to go beyond the resonance region to avoid possible interference effects. On the other hand, as we have seen in the results of Fig. 9, the beam asymmetry can impose constraints on the $NN\eta$ coupling constant that are much more stringent than the differential cross sections because of the interference between the nucleonic and resonance currents. One difficulty of the present calculation is to reproduce the $\sin(2\theta_\eta)$ dependence exhibited by the measured target asymmetry near threshold and this shows that further investigations are necessary to understand better the production mechanism of this reaction.

Our model can also explain the available data on $\pi^- p \to n\eta$ reasonably well, at least for energies not too far from the threshold. At higher energies the total cross section is underestimated due to the lack of the $N\pi\pi$ contribution via the coupled channel.

Our model also describes the $NN \to NN\eta$ reaction data rather well. This is in contrast to the results of Ref. [26], where the pp and $p\eta$ invariant mass distributions are well-described but the $pp\eta$ total cross section is underestimated by a factor as large as about 5 near threshold. This problem has been cured to a large extent in the present approach. However, we still underestimate the total cross section by a factor of ~ 1.5 in the region of $Q \leq 10$ MeV, which is expected to be addressed once the $N\eta$ FSI and three-body effects are properly taken into account. We also verified that the analyzing power is sensitive to the reaction dynamics. Unfortunately, however, the currently available data are not accurate enough to unambiguously distinguish different dynamical contributions.

As we have illustrated with some selected examples, the present approach is unable to determine a unique set of (resonance) parameter values. In fact, it was shown that different parameter sets which describe the data equally well lead to results which exhibit quite different reaction dynamics. This is especially true for the $NN \to NN\eta$ reaction, where we found quite different values of the RNV coupling constants. The inclusion of vector-meson production reactions into the combined analysis should help constrain those coupling constants. Consequently, our study reveals that one must be cautious in interpreting the resonance parameters extracted from this kind of analyses, especially, if only a single reaction process is considered. It is clear that in order to extract more accurate information on the nucleon resonances, one must combine the investigation of hadron-induced meson production with the corresponding photon-induced reactions. To help in this, ample data sets are now available for photo- and electroproduction processes from various accelerator facilities including the Thomas Jefferson National Accelerator Facility, SPring-8, CB/ELSA, GRAAL, etc. By contrast, data for hadron-induced production processes are much more limited and we clearly need more of them.

In this connection, we note that the progress in the study of meson-production processes in NN collisions, both experimentally and theoretically, has reached such a level that it allows us to address certain concrete physics issues, especially, when they are investigated in conjunction with other independent reactions. This has been illustrated in the present work for the specific case of η production where some information on nucleon resonances can be extracted. In particular, the consideration of meson-production processes in NN collisions in conjunction with photon- and (two-body) hadron-induced reactions aiming at a resonance parameters extraction, should help impose more stringent constraints on these parameters. As pointed out in the last subsection, meson production in NN collisions exhibit much richer interference effects, a feature that is absent in more basic two-body reactions. Furthermore, the inclusion of this reaction in the resonance-parameter extraction is especially relevant because the existing data for meson production (other than for the pion) in two-body hadronic reactions are rather scarce and of relatively low accuracy. Currently, there exist only very limited efforts to improve or extend the corresponding database [28]. On the other hand, the available data on meson production in NN collisions are much more accurate and, moreover, the corresponding database can be and is being expanded, especially at the COSY facility.

Acknowledgments

This work was partly supported by the Forschungszentrum Jülich under FFE Grant No. 41445282, the U.S. National Science Foundation under Grant No. PHY-0457265, and the Welch Foundation under Grant No. A-1358. One of us (K.N.) gratefully acknowledges the warm hospitality of the Center for Nuclear Studies of The George Washington University during his visit.

APPENDIX

In this Appendix we give the ingredients which define our models described in Sec. II. Throughout this paper, we use the notation N and R for the nucleon

and nucleon resonance fields, respectively; M_B denotes the mass of the baryon B $(= N, R)$. We also use S $(= \sigma, \vec{a}_0)$, P $(= \eta, \vec{\pi})$, and V_μ $(= \omega_\mu, \vec{\rho}_\mu)$ to denote the scalar, pseudoscalar, and vector meson fields, respectively. The vector notation refers to the isospin space. For isovector mesons, $S \equiv \vec{S}\cdot\vec{\tau}$, $P \equiv \vec{P}\cdot\vec{\tau}$, and $V_\mu \equiv \vec{V}_\mu\cdot\vec{\tau}$. The mass of the meson M is denoted by M_M $(M = S, P, V)$. The photon field is denoted by A_μ. We define $V^{\mu\nu} \equiv \partial^\mu V^\nu - \partial^\nu V^\mu$ and $F^{\mu\nu} \equiv \partial^\mu A^\nu - \partial^\nu A^\mu$.

We use the superscript j^P in the Lagrangian densities ($\mathcal{L}^{(j^P)}$) involving the nucleon resonance R to denote the spin-parity j^P of that resonance. Furthermore, for convenience, we define

$$\Gamma^{(+)} \equiv \gamma_5 \qquad \text{and} \qquad \Gamma^{(-)} \equiv 1\ . \tag{A.1}$$

1. Hadronic interaction Lagrangians

The following interaction Lagrangian densities describe the hadronic vertices. The Lagrangians for meson-nucleon interactions are

$$\mathcal{L}_{NNS} = g_{NNS}\,\bar{N}NS, \tag{A.2}$$

$$\mathcal{L}_{NNP} = -g_{NNP}\,\bar{N}\left\{\Gamma^{(+)}\left[i\lambda + \frac{1-\lambda}{2M_N}\partial\!\!\!/\right]P\right\}N, \tag{A.3}$$

$$\mathcal{L}_{NNV} = -g_{NNV}\,\bar{N}\left\{\left[\gamma^\mu - \kappa_V\frac{\sigma^{\mu\nu}\partial_\nu}{2M_N}\right]V_\mu\right\}N, \tag{A.4}$$

where the parameter λ was introduced in $\mathcal{L}_{NNP}$ to interpolate between the pseudovector ($\lambda = 0$) and the pseudoscalar ($\lambda = 1$) couplings.

The effective Lagrangians describing the interactions of nucleon resonance with the nucleon and pseudoscalar meson P or vector meson V read

$$\mathcal{L}^{(\frac{1}{2}^\pm)}_{RNP} = \mp g_{RNP}\bar{R}\left\{\Gamma^{(\pm)}\left[i\lambda + \frac{1-\lambda}{M_R \pm M_N}\partial\!\!\!/\right]P\right\}N + \text{ H. c.}, \tag{A.5}$$

$$\mathcal{L}^{(\frac{1}{2}^\pm)}_{RNV} = -\frac{1}{2M_N}\bar{R}\Gamma^{(\mp)}\left\{\left[g_{RNV}\left(\frac{\gamma_\mu\partial^2}{M_R \mp M_N} - i\partial_\mu\right) - f_{RNV}\sigma_{\mu\nu}\partial^\nu\right]V^\mu\right\}N + \text{ H. c.}, \tag{A.6}$$

for a resonance of spin-$\frac{1}{2}$. The Lagrangian (A.5) contains the pseudoscalar-pseudovector mixing parameter λ, similar to Eq. (A.3).

For spin-$\frac{3}{2}$ resonances, we use

$$\mathcal{L}^{(\frac{3}{2}^\pm)}_{RNP} = \frac{g_{RNP}}{M_P}\bar{R}^\mu\Theta_{\mu\nu}(z)\Gamma^{(\pm)}(\partial^\nu P)N + \text{ H. c.}, \tag{A.7}$$

$$\mathcal{L}^{(\frac{3}{2}^\pm)}_{RNV} = -i\frac{g^{(1)}_{RNV}}{2M_N}\bar{R}^\beta\Theta_{\beta\mu}\Gamma^{(\pm)}\gamma_\nu V^{\mu\nu}N - \frac{g^{(2)}_{RNV}}{4M_N^2}\bar{R}^\beta\Theta_{\beta\mu}\Gamma^{(\pm)}V^{\mu\nu}\partial_\nu N \mp \frac{g^{(3)}_{RNV}}{4M_N^2}\bar{R}^\beta\Theta_{\beta\mu}\Gamma^{(\pm)}\left(\partial_\nu V^{\mu\nu}\right)N + \text{ H. c.}, \tag{A.8}$$

where the coupling tensor is $\Theta_{\mu\nu} = g_{\mu\nu} - (z + \frac{1}{2})\gamma_\mu\gamma_\nu$ and we take the off-shell parameter $z = -\frac{1}{2}$ for simplicity.

For the interaction Lagrangians of spin-$\frac{5}{2}$ resonances, we use

$$\mathcal{L}^{(\frac{5}{2}^\pm)}_{RNP} = i\frac{g_{RNP}}{M_P^2}\bar{N}\Gamma^{(\pm)}\left(\partial^\mu\partial^\nu P\right)R_{\mu\nu} + \text{ H. c.}, \tag{A.9}$$

$$\mathcal{L}^{(\frac{5}{2}^\pm)}_{RNV} = \frac{g^{(1)}_{RNV}}{(2M_N)^2}\bar{N}\gamma_\nu\Gamma^{(\mp)}\left(\partial^\alpha V^{\mu\nu}\right)R_{\mu\alpha} - i\frac{g^{(2)}_{RNV}}{(2M_N)^3}(\partial_\nu\bar{N})\Gamma^{(\mp)}\left(\partial^\alpha V^{\mu\nu}\right)R_{\mu\alpha} + i\frac{g^{(3)}_{RNV}}{(2M_N)^3}\bar{N}\Gamma^{(\mp)}\left(\partial^\alpha\partial_\nu V^{\mu\nu}\right)R_{\mu\alpha} + \text{ H. c.}, \tag{A.10}$$

The hadronic interaction Lagrangians among mesons are

$$\mathcal{L}_{\rho\rho\eta} = -\frac{g_{\rho\rho\eta}}{2M_\rho}\varepsilon_{\alpha\beta\nu\mu}(\partial^\alpha\vec{\rho}^\beta)\cdot(\partial^\nu\vec{\rho}^\mu)\eta\ , \tag{A.11a}$$

$$\mathcal{L}_{\omega\omega\eta} = -\frac{g_{\omega\omega\eta}}{2M_\omega}\varepsilon_{\alpha\beta\nu\mu}(\partial^\alpha\omega^\beta)(\partial^\nu\omega^\mu)\eta\ , \tag{A.11b}$$

$$\mathcal{L}_{\pi\eta a_0} = \frac{g_{\pi\eta a_0}}{\sqrt{M_\pi M_\eta}}(\partial_\mu\eta)(\partial^\mu\vec{\pi})\cdot\vec{a}_0\ , \tag{A.11c}$$

with the convention $\varepsilon_{0123} = -1$ for the Levi-Civita antisymmetric tensor.

We follow Refs. [20, 38] for the coupling constant values at the NNM vertices above, except for the coupling constant $g_{NN\eta}$, which is treated as a free parameter in the present work. The coupling constants of the RNM interaction Lagrangians, as well as the resonance masses M_R, are free parameters to be adjusted to reproduce the data. For the other coupling constants, following Ref. [20], we use $g_{\eta\rho\rho} = 4.94$, $g_{\eta\omega\omega} = 4.84$, and $g_{\eta\pi a_0} = 1.81$.

2. Electromagnetic interaction Lagrangians

The electromagnetic vertices are calculated from the Lagrangian densities given below. The electromagnetic interaction of the nucleon reads

$$\mathcal{L}_{NN\gamma} = -e\bar{N}\left\{\left[\hat{e}\gamma^\mu - \hat{\kappa}\frac{\sigma^{\mu\nu}\partial_\nu}{2M_N}\right]A_\mu\right\}N, \tag{A.12}$$

where e stands for the elementary charge unit, and $\hat{e} \equiv (1+\tau_3)/2$ and $\hat{\kappa} \equiv \kappa_p(1+\tau_3)/2 + \kappa_n(1-\tau_3)/2$, with the anomalous magnetic moments $\kappa_p = 1.739$ of the proton and $\kappa_n = -1.931$ of the neutron.

The photo-transition Lagrangians of resonances into the nucleon are

$$\mathcal{L}^{(\frac{1}{2}^\pm)}_{RN\gamma} = e\frac{g^{(1)}_{RN\gamma}}{2M_N}\bar{R}\Gamma^{(\mp)}\sigma_{\mu\nu}\partial^\nu A^\mu N + \text{ H. c.}, \tag{A.13}$$

$$\mathcal{L}^{(\frac{3}{2}^\pm)}_{RN\gamma} = -ie\frac{g^{(1)}_{RN\gamma}}{2M_N}\bar{R}^\beta\Theta_{\beta\mu}\Gamma^{(\pm)}\gamma_\nu F^{\mu\nu}N - e\frac{g^{(2)}_{RN\gamma}}{4M_N^2}\bar{R}^\beta\Theta_{\beta\mu}\Gamma^{(\pm)}F^{\mu\nu}\partial_\nu N + \text{ H. c.}, \tag{A.14}$$

$$\mathcal{L}^{(\frac{5}{2}^\pm)}_{RN\gamma} = e\frac{g^{(1)}_{RN\gamma}}{(2M_N)^2}\bar{N}\gamma_\nu\Gamma^{(\mp)}\left(\partial^\alpha F^{\mu\nu}\right)R_{\mu\alpha} - ie\frac{g^{(2)}_{RN\gamma}}{(2M_N)^3}(\partial_\nu\bar{N})\Gamma^{(\mp)}\left(\partial^\alpha F^{\mu\nu}\right)R_{\mu\alpha} + \text{ H. c.}, \tag{A.15}$$

and the photo-transition Lagrangian between mesons are

$$\mathcal{L}_{\eta\rho\gamma} = -e\frac{g_{\eta\rho\gamma}}{M_\rho}\varepsilon_{\alpha\beta\nu\mu}(\partial^\alpha\rho_0^\beta)(\partial^\nu A^\mu)\eta, \tag{A.16a}$$

$$\mathcal{L}_{\eta\omega\gamma} = -e\frac{g_{\eta\omega\gamma}}{M_\omega}\varepsilon_{\alpha\beta\nu\mu}(\partial^\alpha\omega^\beta)(\partial^\nu A^\mu)\eta. \tag{A.16b}$$

The electromagnetic coupling constants involving nucleon resonances in the above Lagrangians are free parameters to be adjusted to fit the pertinent experimental data. The coupling constants $g_{\eta v\gamma}$ ($v = \rho, \omega$) in the above equations are determined from a systematic analysis of the pseudoscalar and vector meson radiative decays [20, 52], which leads to $g_{\eta\rho\rho} = 1.44$ and $g_{\eta\omega\omega} = 0.47$. Their signs are inferred also from $SU(3)$ flavor symmetry considerations in conjunction with the sign of the coupling constant $g_{\pi v\gamma}$ determined from a study of pion photoproduction in the 1 GeV energy region [53].

3. Form Factors

Each vertex obtained from the interaction Lagrangians given above is multiplied by a phenomenological cutoff function

$$F(p'^2, p^2, q^2) = F_B(p'^2)F_B(p^2)F_M(q^2), \tag{A.17}$$

where p' and p denote the four-momenta of the two baryons, and q is the four-momentum of the meson at the three-point vertex. Here, we use

$$F_B(x) = \frac{\Lambda_B^4}{\Lambda_B^4 + (x - M_B^2)^2}, \tag{A.18}$$

where the cutoff $\Lambda_B = 1200$ MeV is taken the same for all the baryons, and $F_M(q^2)$ is given by

$$F_M(q^2) = \left(\frac{\Lambda_M^2 - M_M^2}{\Lambda_M^2 - q^2}\right)^n, \tag{A.19}$$

with $n = 1$ for a scalar or a pseudoscalar meson and $n = 2$ for a vector meson. The values of Λ_M are taken the same as those used in Ref. [20].

The electromagnetic $\eta v\gamma$ vertex is multiplied by the form factor $G_v(q^2)$ which describes the off-shell behavior of the intermediate vector meson with squared momentum transfer q^2 (cf. the fourth diagram in Fig. 1). In general, we use the dipole form

$$G_v(q^2) = \left(\frac{\Lambda_v^{*2}}{\Lambda_v^{*2} - q^2}\right)^2, \tag{A.20}$$

where the cutoff Λ_v^*, taken to be same for both ρ and ω, is a free parameter.

4. Propagators

The calculation of the Feynman diagrams displayed in Figs. 1, 2, and 3 requires the corresponding baryon and meson propagators. Their explicit forms are given here.

$$S(p) = \frac{1}{\not{p} - M_N + i\epsilon} \ , \tag{A.21}$$

$$\Delta(q^2) = \frac{1}{q^2 - M_M^2 + i\epsilon} \ , \tag{A.22}$$

$$D^{\mu\nu}(q) = \frac{-g^{\mu\nu} + q^\mu q^\nu / M_V^2}{q^2 - M_V^2 + i\epsilon} \ , \tag{A.23}$$

where $S(p)$ is the nucleon propagator with the nucleon four-momentum p, $\Delta(q^2)$ is the scalar or pseudoscalar meson propagator with four-momentum q, and $D^{\mu\nu}(q)$ is the vector meson propagator.

For a spin-1/2 resonance propagator, we use the ansatz

$$\begin{aligned} S_{1/2}(p) &= \frac{1}{\not{p} - M_R + \frac{i}{2}\Gamma} \\ &= \frac{\not{p} + M_R}{p^2 - M_R^2 + \frac{i}{2}(\not{p} + M_R)\Gamma} \ , \end{aligned} \tag{A.24}$$

where Γ is the energy dependent resonance width.

For spin-3/2, the resonant propagator reads in a schematic matrix notation

$$S_{3/2}(p) = \left[(\not{p} - M_R) g - i \frac{\Delta}{2} \Gamma \right]^{-1} \Delta \ , \tag{A.25}$$

where all indices are suppressed, i.e., g is the metric tensor and Δ is the Rarita-Schwinger tensor written in full detail as

$$\Delta^{\mu\nu}_{\beta\alpha} = -g^{\mu\nu}\delta_{\beta\alpha} + \frac{1}{3}\gamma^\mu_{\beta\varepsilon}\gamma^\nu_{\varepsilon\alpha} + \frac{2p^\mu p^\nu}{3M_R^2}\delta_{\beta\alpha} + \frac{\gamma^\mu_{\beta\alpha}p^\nu - p^\mu\gamma^\nu_{\beta\alpha}}{3M_R}, \tag{A.26}$$

where α, β, and ε enumerate the four indices of the γ-matrix components (summation over ε is implied). The inversion in Eq. (A.25) is to be understood on the full 16-dimensional space of the four Lorentz indices and the four components of the gamma matrices. The motivation for the ansatz (A.25) and the technical details how to perform this inversion is given in Ref. [38].

Similarly, the propagator for a spin-5/2 resonance is given by

$$S_{5/2}(p) = \left[(\not{p} - M_R) g - i \frac{G}{2} \Gamma \right]^{-1} G. \tag{A.27}$$

where

$$\begin{aligned} G \equiv G^{\mu\nu;\rho\tau}_{\beta\alpha} &= \left[\frac{1}{2} \left(\bar{g}^{\mu\rho}\bar{g}^{\nu\tau} + \bar{g}^{\mu\tau}\bar{g}^{\nu\rho} \right) - \frac{1}{5}\bar{g}^{\mu\nu}\bar{g}^{\rho\tau} \right] \delta_{\beta\alpha} \\ &- \frac{1}{10} \left(\bar{g}^{\mu\rho}\bar{\gamma}^\nu_{\beta\varepsilon}\bar{\gamma}^\tau_{\varepsilon\alpha} + \bar{g}^{\mu\tau}\bar{\gamma}^\nu_{\beta\varepsilon}\bar{\gamma}^\rho_{\varepsilon\alpha} + \bar{g}^{\nu\rho}\bar{\gamma}^\mu_{\beta\varepsilon}\bar{\gamma}^\tau_{\varepsilon\alpha} + \bar{g}^{\nu\tau}\bar{\gamma}^\mu_{\beta\varepsilon}\bar{\gamma}^\rho_{\varepsilon\alpha} \right), \end{aligned} \tag{A.28}$$

with

$$\bar{g}^{\mu\nu} \equiv g^{\mu\nu} - \frac{p^\mu p^\nu}{M_R^2}, \qquad \bar{\gamma}^\mu \equiv \gamma^\mu - \frac{p^\mu \not{p}}{M_R^2}. \tag{A.29}$$

The above spin-5/2 propagator is a variant of the one given in Ref. [54].

We write the resonance width Γ as a function of $W = \sqrt{s}$ according to

$$\Gamma(W) = \Gamma_R \left[\sum_{i=1}^{N} \beta_i \hat{\Gamma}_i(W) + \sum_{j=1}^{N_\gamma} \gamma_j \hat{\Gamma}_{\gamma_j}(W) \right], \tag{A.30}$$

where the sums over i and j respectively account for decays of the resonance into N and two- or three-hadron channels and into N_γ radiative decay channels. The total static resonance width is denoted by Γ_R and the numerical factors β_i and γ_j (with $0 \le \beta_i, \gamma_j \le 1$) describe the branching ratios into the corresponding decay channel, i.e.,

$$\sum_{i=1}^{N} \beta_i + \sum_{j=1}^{N_\gamma} \gamma_j = 1. \tag{A.31}$$

We parametrize the width functions $\hat{\Gamma}_i$ and $\hat{\Gamma}_{\gamma_j}$ (which are both normalized to 1 at $W = M_R$) as given in Ref. [38] to provide the correct respective threshold behavior.

[1] O. Bartalini *et al.* (GRAAL Collaboration), Eur. Phys. J. A **33**, 169 (2007); O. Bartholomy *et al.* (CB-ELSA Collaboration), Eur. Phys. J. A **33**, 133 (2007); T. Nakabayashi *et al.*, Phys. Rev. C **74**, 035202 (2006); V. Credé *et al.* (CB-ELSA Collaboration), Phys. Rev. Lett. **94**, 012004 (2005); M. Dugger *et al.* (CLAS Collaboration), Phys. Rev. Lett. **89**, 222002 (2002); B. Krusche *et al.*, Phys. Rev. Lett. **74**, 3736 (1995).

[2] D. Elsner *et al.* (CBELSA/TAPS Collaboration), Eur. Phys. J. **A33**, 147 (2007); V. Kuznetsov *et al.*, in *Proceedings of the 9th International Symposium on Meson-Nucleon Physics and the Structure of the Nucleon, MENU2001 (July 26–31, 2001, Washington, DC)*, edited by H. Haberzettl and W.J. Briscoe [πN Newsletter **16**, 160 (2002)]; J. Ajaka *et al.*, Phys. Rev. Lett. **81**, 1797 (1998); A. Bock *et al.*, Phys. Rev. Lett. **81**, 534 (1998).

[3] V. Kuznetsov *et al.*, Phys. Lett. **B647**, 23 (2007).

[4] V. Kuznetsov *et al.*, arXiv:hep-ex/0703003; L. Tiator,

Int. J. Mod. Phys. A **22**, 297 (2007); A. Fix, L. Tiator, and M. Polyakov, Eur. Phys. J. A **32**, 311 (2007); V. Shklyar, A. Lenske, and U. Mosel, Phys. Lett. **B650**, 172 (2007); K.-S. Choi, S. I. Nam, A. Hosaka, and H.-C. Kim, arXiv:0707.3854; Phys. Lett. **B636**, 253 (2006).

[5] H. Shimizu, Talk at the International Workshop on the Physics of Excited Baryons (NSTAR2007), Bonn, Germany, September 5–8, 2007, `http://nstar2007.uni-bonn.de`.

[6] I. Jaegle (for the CBELSA-TAPS Collaboration), in *Proceedings of the Workshop on the Physics of Excited Nucleons (NSTAR2005), Tallahassee, October 12–15, 2005*, edited by S. Capstick, V. Credé, and P. Eugenio, (World Scientific, Singapore, 2006) pp. 340–344; H. Schmieden, Talk at the International Workshop on the Physics of Excited Baryons (NSTAR2007), Bonn, Germany, September 5–8, 2007, `http://nstar2007.uni-bonn.de`.

[7] See, for example, R. A. Arndt, Ya. I. Azimov, M. V. Polyakov, I. I. Strakovsky, and R. L. Workman, Phys. Rev. C **69**, 035208 (2004); D. Diakonov and V. Petrov, Phys. Rev. D **69**, 094011 (2004); Y. Oh, H. Kim, and S. H. Lee, Phys. Rev. D **69**, 094009 (2004).

[8] V. A. Tryasuchev, Eur. Phys. J. A **22**, 97 (2004); I. G. Aznauryan, Phys. Rev. C **68**, 065204 (2003); B. Borasoy, E. Marco, and S. Wetzel, Phys. Rev. C **66**, 055208 (2002); E. V. Balandina, E. M. Leĭkin, and N. P. Yudin, Yad. Fiz. **65**, 1755 (2002) [Phys. Atom. Nucl. **65**, 1711 (2002)]; R. Workman, R. A. Arndt, and I. I. Strakovsky, Phys. Rev. C **62**, 048201 (2000); L. Tiator, D. Drechsel, G. Knochlein, and C. Bennhold, Phys. Rev. C **60**, 035210 (1999); N. C. Mukhopadhyay and N. Mathur, Phys. Lett. **B444**, 7 (1998); C. Deutsch-Sauermann, B. Friman, and W. Nörenberg, Phys. Lett. **B409**, 51 (1997); B. Krusche, N. C. Mukhopadhyay, J. F. Zhang, and M. Benmerrouche, Phys. Lett. **B397**, 171 (1997); N. Kaiser, T. Waas, and W. Weise, Nucl. Phys. **A612**, 297 (1997); N. C. Mukhopadhyay, J. F. Zhang, and M. Benmerrouche, Phys. Lett. **B364**, 1 (1995); M. Benmerrouche, N. C. Mukhopadhyay, and J. F. Zhang, Phys. Rev. D **51**, 3237 (1995); M. Benmerrouche and N. C. Mukhopadhyay, Phys. Rev. Lett. **67**, 1070 (1991); C. Gobbi, A. Hosaka, and N. Scoccola, Nucl. Phys. **A562**, 461 (1993).

[9] L. Tiator, C. Bennhold, and S. S. Kamalov, Nucl. Phys. **A580**, 455 (1994).

[10] S. D. Bass, S. Wetzel, and W. Weise, Nucl. Phys. **A686**, 429 (2001).

[11] C. Fernandez-Ramirez, E. Moya de Guerra, and J. M. Udias, Phys. Lett. **B651**, 369 (2007).

[12] W.-T. Chiang, S. N. Yang, L. Tiator, M. Vanderhaeghen, and D. Drechsel, Phys. Rev. C **68**, 045202 (2003); W.-T. Chiang, S. N. Yang, L. Tiator, and D. Drechsel, Nucl. Phys. **A700**, 429 (2002).

[13] A. V. Anisovich *et al.*, Eur. Phys. J. A **25**, 427 (2005).

[14] J. He, B. Saghai, and Z. Li, arXiv:0802.3816; B. Saghai and Z. Li, Eur. Phys. J. A **11**, 217 (2001); Z. Li and B. Saghai, Nucl. Phys. **A644**, 345 (1998).

[15] W. M. Yao *et al.* (Particle Data Group), J. Phys. G **33**, 1 (2006).

[16] P. Moskal *et al.*, Phys. Lett. **B474**, 416 (2000); B. Tatischeff *et al.*, Phys. Rev. C **62**, 054001 (2000); H. Calén *et al.*, Phys. Lett. **B458**, 190 (1999); H. Calén *et al.*, Phys. Rev. C **58**, 2667 (1998); F. Hibou *et al.*, Phys. Lett. **B438**, 41 (1998); H. Calén *et al.*, Phys. Rev. Lett. **80**, 2069 (1998); H. Calén *et al.*, Phys. Rev. Lett. **79**, 2642 (1997); H. Calén *et al.*, Phys. Lett. **B366**, 39 (1996); E. Chiavassa *et al.*, Phys. Lett. **B322**, 270 (1994).

[17] M. Abdel-Bary *et al.* (COSY-TOF Collaboration), Eur. Phys. J. A **16**, 127 (2003).

[18] P. Moskal *et al.*, Phys. Rev. C **69**, 025203 (2004).

[19] R. Czyzykiewicz *et al.*, Phys. Rev. Lett. **98**, 122003 (2007); P. Winter *et al.*, Phys. Lett. **B544** 251 (2002), **B553**, 339(E) (2003); P. Moskal *et al.*, Phys. Lett. **B482**, 356 (2000).

[20] K. Nakayama, J. Speth, and T-.S. H. Lee, Phys. Rev. C **65**, 045210 (2002).

[21] C. Hanhart, Phys. Rept. **397**, 155 (2004).

[22] S. Ceci, A. Švarc, and B. Zauner, Phys. Scripta **73**, 663 (2006).

[23] V. Baru *et al.*, Phys. Rev. C **67**, 024002 (2003).

[24] A. Fix and H. Arenhövel, Phys. Rev. C **69**, 014001 (2004).

[25] A. Deloff, Phys. Rev. C **69**, 035206 (2004).

[26] K. Nakayama, J. Haidenbauer, C. Hanhart, and J. Speth, Phys. Rev. C **68**, 045201 (2003).

[27] T. Morrison, Ph.D. Thesis, The George Washington University (1999); R. M. Brown *et al.*, Nucl. Phys. **B153**, 89 (1979); N. C. Debenham *et al.*, Phys. Rev. D **12**, 2545 (1975); J. Feltesse *et al.*, Nucl. Phys. **B93**, 242 (1975); B. W. Richards *et al.*, Phys. Rev. D **1**, 10 (1970); F. Bulos *et al.*, Phys. Rev. **187**, 1827 (1969); W. Deinet *et al.*, Nucl. Phys. **B11**, 495 (1969); F. Bulos *et al.*, Phys. Rev. Lett. **13**, 486 (1964); all data are available in the SAID database at `http://gwdac.phys.gwu.edu`.

[28] S. Prakhov *et al.*, Phys. Rev. C **72**, 015203 (2005).

[29] C. Bennhold and H. Tanabe, Phys. Lett. **B243**, 13 (1990).

[30] T. Inoue, E. Oset, and M. J. Vicente-Vacas, Phys. Rev. C **65**, 035204 (2002).

[31] G. Penner and U. Mosel, Phys. Rev. C **66**, 055211 (2002).

[32] A. Gasparyan, J. Haidenbauer, C. Hanhart, and J. Speth, Phys. Rev. C **68**, 045207 (2003).

[33] S. Ceci, A. Švarc, and B. Zauner, Phys. Rev. Lett. **97**, 062002 (2006).

[34] A. Matsuyama, T. Sato, and T.-S. H. Lee, Phys. Rept. **439**, 193 (2007).

[35] X.-H. Zhong, Q. Zhao, J. He, and B. Saghai, Phys. Rev. C **76**, 065205 (2007).

[36] B. Krippa, Phys. Rev. C **64**, 047602 (2001).

[37] R. A. Arndt *et al.*, Phys. Rev. C **72**, 045202 (2005).

[38] K. Nakayama and H. Haberzettl, Phys. Rev. C **69**, 065212 (2004); Phys. Rev. C **73**, 045211 (2006).

[39] H. Haberzettl, K. Nakayama, and S. Krewald, Phys. Rev. C **74**, 045202 (2006).

[40] H. Haberzettl, Phys. Rev. C **56**, 2041 (1997).

[41] H. Haberzettl, C. Bennhold, T. Mart, and T. Feuster, Phys. Rev. C **58**, R40 (1998).

[42] R. M. Davidson and R. Workman, Phys. Rev. C **63**, 025210 (2001).

[43] K. Nakayama, A. Szczurek, C. Hanhart, J. Haidenbauer, and J. Speth, Phys. Rev. C **57**, 1580 (1998).

[44] M. Lacombe *et al.*, Phys. Rev. C **21**, 861 (1980).

[45] K. Nakayama, H. Arellano, J. Durso, and J. Speth, Phys. Rev. C **65**, 045210 (2002).

[46] V. Kuznetsov *et al.*, arXiv:0801.0778.

[47] K. Nakayama and W. G. Love, Phys. Rev. C **70**, 012201 (2004); Phys. Rev. C **72**, 034603 (2005).

[48] R. A. Arndt, W. J. Briscoe, I. I. Strakovsky, and R. L.

Workman, Phys. Rev. C **74**, 045205 (2006).
[49] O. Krehl, C. Hanhart, S. Krewald, and J. Speth, Phys. Rev. C **62**, 025207 (2000).
[50] K. Tsushima and K. Nakayama, Phys. Rev. C **68**, 034612 (2003); K. Nakayama, J. W. Durso, J. Haidenbauer, C. Hanhart, and J. Speth, Phys. Rev. C **60**, 055209 (1999); Y. Oh and T.-S. H. Lee, Phys. Rev. C **69**, 025201 (2004); Nucl. Phys. **A721**, 743 (2003); Phys. Rev. C **66**, 045201 (2002); Y. Oh, A. I. Titov, and T.-S. H. Lee, Phys. Rev. C **63**, 025201 (2001); in *Proceedings of the Workshop on Excited Nucleons and Hadronic Structure (NSTAR2000)*, edited by V. D. Burkert, L. Elouadrhiri, J. J. Kelly, and R. C. Minehart, (World Scientific, Singapore, 2000); arXiv:nucl-th/0004055.
[51] Ch. Pauly, Ph.D. Thesis, University of Hamburg (2006).
[52] J. W. Durso, Phys. Lett. **B184**, 348 (1987).
[53] H. Garcilazo and E. Moya de Guerra, Nucl. Phys. **A562**, 521 (1993).
[54] S.-J. Chang, Phys. Rev. **161**, 1308 (1967); J. G. Rushbrooke, Phys. Rev. **143**, 1345 (1966); R. E. Behrends and C. Fronsdal, Phys. Rev. **106**, 345 (1957).